TUTORIAL REVIEW

Check for updates

Insights into the role of transition and noble metals mediating photochemical vapor generation†

Ralph E. Sturgeon, [ID] *[a] Enea Pagliano, [ID] [a] Gisele S. Lopes, [ID] [b] Renato S. A. Neto[b] and Jane K. S. Brito[b]

The recent expansion of the suite of elements amenable to photochemical vapor generation (PVG) is primarily linked to the addition of mg L^{-1} concentrations of selected transition metals (TMs) to the photolysis medium, principally Fe, Cd, Co, Ni and Cu. Their presence enhances synthesis yields of several analytical targets, particularly carbonylated species, in some cases by orders of magnitude. A consideration of curated analytical PVG literature reveals substantial inconsistencies with the current use of generalized ligand-to-metal charge transfer processes to mechanistically account for these so-called TM "sensitizer" effects *via* their enhancement in free radical populations participating in the PVG synthesis routes. In this study, a novel approach utilizes an independent window for evaluation of the effects of added TMs on radical production based on an examination of the altered concentration profiles of H_2, CO, CH_4 and CO_2 generated in formic and acetic acid media, whose origins lie with the precursor free radicals responsible for the analytical PVG process. A photocatalytic mechanism induced by homogeneous co-generation of TM nanoparticles is proposed which more reasonably accounts for both the altered gas profiles and their notable selectivity evident with improved PVG efficiencies of specific analytes. A tutorial approach to the topic has been adopted in an effort to provide a balanced framework within which the various processes are comprehensively discussed with relevance to state-of-the-art PVG techniques and current literature.

[a]Metrology Research Center, National Research Council Canada, Inorganic Chemistry, Ottawa, Canada K1A 0R6. E-mail: Ralph.sturgeon@nrc-cnrc.gc.ca

[b]Departamento de Química Analítica e Físico-Química, Centro de Ciencias, Campus do Pici, Universidade Federal do Ceara, Fortaleza, CE, Brazil

† Presented at the 16th Rio Symposium on Atomic Spectrometry, Bento Gonçalves, Brazil, November 28–30, 2023.
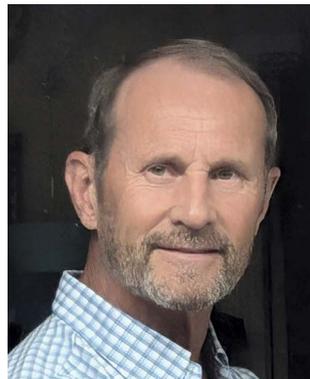
Ralph Sturgeon obtained his PhD is 1977 and has been with the National Research Council of Canada, Ottawa since that time and is currently an Emeritus Researcher. His interests lie in trace element analysis, vapor generation, organometallic speciation and production of Certified Reference Materials with a focus on atomic and mass spectrometric detection techniques. The fundamentals of vapor generation techniques currently occupy his attention.

Ralph E. Sturgeon

Enea Pagliano completed his PhD studies in analytical chemistry at Scuola Normale Superiore of Pisa and since 2013 has been a research officer at the National Research Council of Canada. Enea is a team member of the Joint Committee for Traceability in Laboratory Medicine, a member of the IUPAC Subcommittee on Metrology in Chemistry, and an adjunct research professor at Carleton University. His research has focused on the development of primary analytical methods for metrological applications.

Enea Pagliano

70 | *J. Anal. At. Spectrom.*, 2025, **40**, 70–97

This journal is © The Royal Society of Chemistry 2025

Introduction

Vapor generation techniques coupled with analytical atomic and mass spectrometry have been in continuous use for more than 50 years.[1] High synthesis yields, improved sample introduction efficiency, inherent matrix separation and enhanced detection power sustain continued interest in both their analytical application and mechanistic understanding. Amongst these, photochemical vapor generation (PVG) is one of the most recent and actively pursued, primarily because of its simplicity, green chemistry, widest scope of application and interest in acquiring a more complete fundamental comprehension of this novel phenomenon; it is currently amenable for analytical use with some 25 elements, including transition and semi-metals as well as the halogens.

The premise of PVG rests on a mechanistic model that the targeted analytes are converted to volatile species during UV irradiation of a (aqueous) medium (typically) containing low molecular weight carboxylic acids (R-COOH; primarily formic and/or acetic, although ethanol has been utilized).[2–5] Emission of UV-C from low pressure Hg discharge sources gives rise to both homolysis of water (induced via 185 nm absorption) and photolysis of the carboxylate anion, yielding both aquated electrons ($e_{(aq)}^-$) as well as a suite of powerful reducing radicals ($H^{\bullet}$, $R^{\bullet}$, and $CO_2^{\bullet-}$). These, and their subsequent thermal reaction products, interact with ionic analytes to ultimately form their volatile free atoms, hydrides, carbonyls or alkylated derivatives, depending on the element and photochemical medium used.

The deleterious presence of concomitant metal cations (and anions such as Cl^- and NO_3^-) in real samples has long been recognized as a primary shortcoming of PVG reactions, leading to interferences often ascribed to radical scavenging effects.[2–4] Nevertheless, it is evident that the most recent advances in PVG have all accrued from use of mg L^{-1} concentrations of select transition metal ions (TMs) deliberately added to reaction media to enhance the yield of many PVG reactions, as summarized in a recent report by Hou and colleagues.[6] Such systems are more appealing (and currently more interesting) than resorting to addition of typically heterogeneous semiconductor (SC) catalysts, such as TiO_2,[7–10] or the use of unique metal organic frameworks (MOFs) which have also improved PVG performance for several elements.[11] A summary of applications of SC catalysts in PVG systems has been presented by Zou et al.[12] but, despite interest, they have enjoyed only limited use.

Gao et al.[13] first highlighted the unique impact of added TMs, noting the addition of a 5 mg L^{-1} concentration of Ni(II) increased the earlier optimized yield of photogenerated lead species 4100-fold. This study was rapidly followed by a succession of publications from many laboratories, which repeatedly confirmed similar efficacious effects, particularly in systems targeting the generation of carbonylated transition metals. For lack of a more informed mechanism of action, the role of these added TMs was putatively designated to be a "sensitizer effect" in early publications. However, the only known occurrence of true sensitization with an organic compound being used for application with PVG has been the use of anthranilic acid as a homogeneous photosensitizer for PVG speciation of mercury.[14] This term should thus be discontinued until the mechanistic aspects of TM mediated reactions are more clearly understood. Additions of Cd(II),[15,16] Co(II),[17–22] Cu(II),[23–25] Fe(II/III),[26–31] Ni(II)[13] and, to a lesser extent, V(IV/V)[32] have been evaluated for both their individual performance characteristics as well as unique synergistic effects arising from their various combinations.[6,33–36] Of equal interest is the sole report of in situ

Gisele S. Lopes is a Full Professor at Universidade Federal do Ceara, Ceara, Brazil. She obtained her PhD in analytical chemistry in 2002 from Universidade Federal de São Carlos, Sao Paulo, Brazil. Her interest lies in analytical chemistry, with emphasis on metrology, trace element analysis, sample preparation and chemometrics.

Gisele S. Lopes

Renato S. A. Neto is currently a PhD student in analytical chemistry at Universidade Federal do Ceara, Ceara, Brazil. He obtained his Master's and Bachelor's degrees from this institution in 2019 and 2017, respectively. His current interest focuses on trace element analysis.

Renato S. A. Neto

Jane K. S. Brito is currently a PhD student in analytical chemistry at Universidade Federal do Ceara, Ceara, Brazil. She obtained her Master's degree in 2021 from Universidade Federal do Ceara and her Bachelor's from Universidade Federal do Piauí, Piauí, Brazil. Her current interest is primarily trace element analysis.
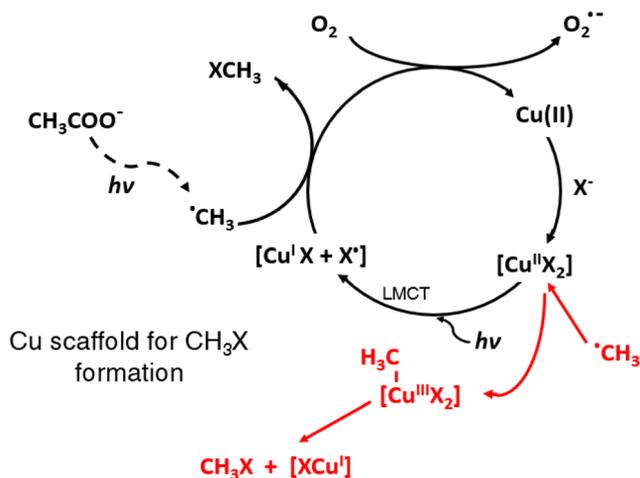
Jane K. S. Brito

This journal is © The Royal Society of Chemistry 2025

J. Anal. At. Spectrom., 2025, 40, 70–97 | 71

Fig. 1 TM-assisted PVG of halogens using added Cu(II) as an example of aquo-metal halide complex formation followed by (i) $^{\cdot}CH_3$ capture of halide atom ($X^{\cdot}$) formed by a LMCT process or (ii, shown in red) oxidative addition of $^{\cdot}CH_3$ to CuX_2 complex followed by reductive elimination of CH_3X and subsequent catalytic re-oxidation of Cu(I) by dissolved oxygen or other oxidants in the system.

formation of nano-CdSe, which promoted reduction of Se(VI) to volatile SeH_2 via irradiation of a sample augmented with 10 mg L^{-1} Cd(II);[37] this finding deserves more extensive study.

Whereas the general role of added TMs functioning in such a "homogeneous" or dissolved manner (as opposed to use of typical SCs or MOFs) is not completely understood at this time, enhanced PVG synthesis of the methylhalogens (XCH_3) from dilute acetic acid containing added TMs[23,25,38] appears to rest on a well-established foundation and likely occurs via either $^{\cdot}CH_3$ capture of $X^{\cdot}$ from its ligand-to-metal charge transfer (LMCT) cage arising from photolysis of an aquated TM-X complex (for I^- and Br^-),[39–41] or by oxidative addition-reductive elimination reactions between $^{\cdot}CH_3$ and the TM-X complex (for Cl^- and F^-). The latter is the most likely mechanism for methylfluoride generation since current photochemical reactors are unable to generate an intermediate charge transfer to solvent (CTTS) cage complex due to source output being limited to >185 nm.[38,42] These scenarios, leading to catalytic cycles, are illustrated in Fig. 1 for the case of a Cu(II)-X complex.

From the broader perspective of general application of TMs beyond the halogens, Sturgeon and colleagues initially proposed a framework for their action based on an augmented production of reducing radicals arising from the photolysis of TM–carboxylate complexes induced by (longer wavelength) LMCT processes.[1,3,4] This, in principle, could enhance PVG reaction kinetics, leading to increased overall analyte generation efficiencies because a broader band of the emission output from the photochemical source could be utilized to produce additional needed radical partners. Such reactions are commonplace in the inorganic and environmental photochemical literature, occurring by exposure of aqueous solutions containing carboxylic acids to UV-B radiation, readily available from solar and low pressure mercury discharge sources.[43,44] Additionally, direct evidence of such enhanced radical production in the presence of added TMs is supported by ESR

spin trapping experiments which confirm elevated (but unquantified) levels of reducing radicals ($CO_2^{\cdot-}$, $^{\cdot}CH_3$) with concurrently decreased concentrations of $^{\cdot}OH$ in irradiated TM-doped PVG reaction media.[6,20,32,45,46] These reports compliment similar such increases earlier noted in classical SC-mediated photochemical systems.[47,48] As a consequence, the LMCT-based mechanism has proliferated, essentially unchallenged, and has become pervasive throughout more recent PVG literature.

The pronounced role of TMs mediating homogeneous PVG reactions likely stems from their d shell configurations which give rise to varied redox properties and multiple oxidation states to serve as scaffolds fostering interaction of reaction partners (cf. Fig. 1). However, an elementary qualitative meta-analysis of the common effects of added TMs published since the first report by Gao et al. in 2015 (ref. 13) readily reveals both trends and inconsistencies with this general LMCT model of action. Most evident is the overwhelming use of Cd, Cu, Fe, Ni and Co for this purpose. As noted above, these elements possess multiple oxidation states and can be readily reduced to their atomic form during PVG. Additionally, with the exception of the halogens, in every experimental system, an optimum concentration of the added TM is evident beyond which higher concentrations lead to reduced PVG yields (this is often ascribed to a "shadowing effect" arising from the filtering and consequent diminished effective intensity of the UV source by TM d–d transitions and charge transfer transitions of TM complexes). Noteworthy, however, is that apart from the halogens the optimal concentration of added TM varies significantly from one targeted analyte system to another, despite otherwise overall identical photoreactor conditions (i.e., same source, same irradiation conditions, ostensibly the same photochemical medium). PVG enhancement yields thus selectively vary considerably from one analyte to another, sometimes by factors of $10–10^3$, despite similar (and often identical) TM concentrations being used, suggesting that there is a specific interaction between the analyte and the added TM. This is further reinforced by the observation that the relative effectiveness of a specific TM added to a given analyte system is often completely different in another analyte system (i.e., analyte specific effects).[6] As well, the existence of combinations of co-added TMs, inducing synergistic effects on analyte response, is both surprising and highly variable; similar to their single element impacts. The most effective combinations of TMs and their relative concentrations beneficial to one analyte are typically unique from those of another analyte[6,33,36] such that no universal combination/concentration can be a priori recommended. Apart from ESR data, these observations occur against a backdrop of increased radical production sometimes visually evident from changes in the rate of generation of stable molecular gases whose precursor species are radicals such as $H^{\cdot}$ and $^{\cdot}CH_3$ arising from the PVG process (as evidenced by enhanced gas bubble segmentation in the liquid outlet line from the photoreactor) when particular TMs are employed.

It appears clear that no single, simple mechanism of action of added TMs, such as the LMTC concept first promulgated by Sturgeon et al.,[1,3,4] can be used to account for the diversity and inconsistency of these observations. As noted by Ford,[49] "…it is

72 | J. Anal. At. Spectrom., 2025, **40**, 70–97

This journal is © The Royal Society of Chemistry 2025

clear that the successful use of inorganic photochemistry, whether in energy science, biomedicine, or other foreseen or unforeseen application, needs to be based on a sound understanding of the fundamental principles that define the mechanisms of these systems…", further experimentation is required to shed light on this phenomenon if knowledgeable use of the phenomenon is to be used to its full advantage. In response to this, an investigation of the relative concentrations of stable small molecules (CO, H_2, CO_2 and CH_4) generated during UV photolysis of acetic and formic acids, and the impact of added TMs on changes to their profiles was undertaken. As these gases are the products of radical precursors arising from direct photolytic and subsequent thermal reactions, this provides a novel independent approach into an examination of the effects of TM mediated PVG on radical production to complement those based on limited ESR detection of these primary radicals. This research is framed within the context of an overarching tutorial review of this subject matter to enhance the perspective of the newly generated results and their interpretation based on a new approach to the mechanism of action of added TMs founded on the production of TM nanoparticles (NPs) possessing intrinsic properties of high chemical and size related selectivity for photochemical reactions.

Experimental

Instrumentation

A 19 W thin-film flow through photoreactor (Beijing Titan Instrument Co. Ltd, Beijing, China) fitted with synthetic quartz conduits (internal volume 0.72 mL) directly embedded in the low pressure mercury discharge exposed aqueous samples to vacuum UV radiation of 185 nm, as described in earlier publications.[13,50,51] Prepared liquid samples were continuously introduced into the photoreactor at 1–2 mL min^{-1}, typical of those used throughout the published PVG literature, using a Gilson Minipuls 2 peristaltic pump (Mandel Scientific, Villiers, Le Bel, France). Effluent from the reactor was directed to a glass thin-film gas–liquid separator (GLS) repurposed from a model 2600 mercury analyzer (Tekran Instruments Corporation, Toronto, Canada).

Liquid waste evacuation from the GLS was accomplished using a separate peristaltic pump. A flow of Ar passing through the GLS in a countercurrent direction to the admitted irradiated sample served to efficiently strip volatile gases from the liquid phase and direct them, *via* a 2 mm i.d. PTFE line, to a 15 cm long (4 mm i.d.) glass dryer tube packed with granular NaOH immobilized between plugs of glass wool. This unit served to remove moisture and acidic vapors. Fresh dryer units were used for each day of measurements. Gas flow was regulated with a calibrated rotameter (Matheson Tri-Gas Inc., Montgomeryville, USA) in line with a precision metering valve and verified for consistency (28 ± 1 mL min^{-1}) at the beginning and end of each set of experiments *via* its rate of volumetric displacement of water. Following passage of the gas stream through the NaOH drying tube, it was directed to 10 mL glass headspace (HS) vials fitted with magnetic ring caps and PTFE/silicone septa seals *via* a short length of 1 mm i.d. tygon line terminating in a 22 gauge luer mounted stainless steel needle. The needle was used to manually pierce septa during gas
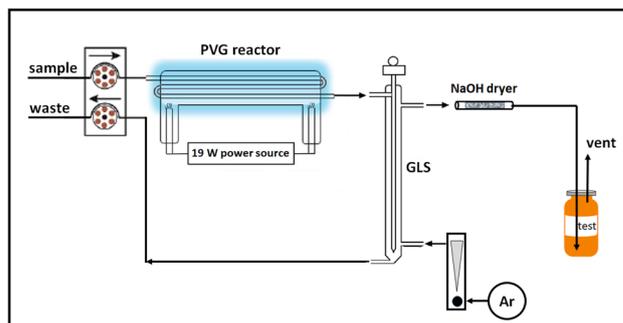

Fig. 2 Schematic of photolysis and gas collection system.

sampling and was inserted to the bottom of the HS vial to ensure efficient flushing of the vial in tandem with a second such needle located just beneath the septum which served as a relief vent to the atmosphere. In this manner excess gas pressure was released to a short length of 2 mm i.d. tygon tubing to ensure a representative HS gas sample. This vent line terminated a few mm below the surface of a water reservoir to ensure no back diffusion of atmospheric gases into the vial occurred during flush/fill operations or after the inlet needle was withdrawn so as to guarantee that the fill pressure in each vial was reproducible and atmospheric, as evidenced by the cessation of bubbling after the input line was removed. Filled vials were transferred to a CTC Analytics PAL RSI autosampler (Zwingen, Switzerland) connected to a double-inlet Agilent 7890A GC system (Santa Clara, CA) equipped with both Agilent TCD and Agilent 7000 TripleQuad mass spectrometry detectors. Before analysis, each sample was incubated at 35 °C for 5 min. Thereafter, a headspace (HS) volume was sampled and injected onto the GC column (syringe held at 40 °C; 4 mm double gooseneck liner held at 200 °C). In all cases, an oven heating program for the chromatography comprised the following: 5 min at 40 °C then 20 °C min^{-1} ramp to 120 °C with a hold for 5 min (14 min run time), followed by rapid cooling in preparation for the next run. A schematic of the irradiation and gas collection system is presented in Fig. 2.

In an effort to prolong the lifetime and ensure reliability of the GC columns, the amount of water and carboxylic acid vapor transfer to the headspace vials was minimized with use of the short column NaOH dryer. More than 90% of acid vapor and water was eliminated with this approach, which unfortunately also significantly ($\sim$92%) adsorbed the CO_2 from the gas stream, necessitating its subsequent determination *via* independent analytical runs which bypassed the dryer column.

A Shimadzu GC-2010 Plus gas chromatograph equipped with a sensitive dielectric barrier discharge ionization detector (DIB) was used for the determination of methanol in irradiated and non-irradiated solutions of 5% (v/v) acetic acid. An identical apparatus and approach to PVG was used as described above. Solid phase microextraction of headspace vapor derived from 1 mL volumes of sample solutions placed in 7 mL glass HS vials sealed with PTFE/silicone septa was manually performed using a SUPELCO assembly comprising a fused silica fiber hosting an 85 μm polyacrylate (PA) coating. Analyte separation was performed on a Shimadzu 30 m × 0.25 mm × 0.25 μm SH-Rtx-Wax column.

This journal is © The Royal Society of Chemistry 2025

J. Anal. At. Spectrom., 2025, **40**, 70–97 | **73**

Reagents and materials

The following materials were all sourced from MilliporeSigma Canada Ltd (Oakville, ON): ACS reagent grade formic (>96%) and glacial acetic (>99.7%) acids, ACS reagent grade ammonium hydroxide (28.0–30.0% NH_3 basis), ACS reagent grade (>99.0%) potassium nitrate, cobalt(II) acetate tetrahydrate (ACS reagent, ≥98.0%), copper(II) acetate monohydrate (ACS reagent, ≥98%), nickel(II) acetate tetrahydrate (98%) and cadmium acetate dihydrate (reagent grade 98%). Concentrated nitric acid was purified in-house by sub-boil distillation. High-purity (18 MΩ cm) water (DIW) was generated in a Milli-Q Advantage system (MilliporeSigma) fed with distilled water and was used for preparation of all test solutions. HPLC grade methanol, sourced from JT Baker (Philadelphia, USA), was used for preparation of calibration standards.

A custom mixture of NIST traceable 1000 ppm (v/v) calibration gases (H_2, CO_2, CO and CH_4) in a balance of 5 N Ar was ordered from Messer Canada Inc. (Mississauga, Ontario Canada).

Procedures

Stock solutions of minimum 5000 mg L^{-1} Cd(II), Co(II), Cu(II) and Ni(II) were prepared in DIW and serially diluted for use as TM additives to test solutions of acetic and formic acids, which were themselves prepared in large batches through volumetric dilution with DIW to yield concentrations in the range 1–20% (v/v). To reliably assess the impact of each experimental parameter, a minimum of 3 to 5 replicate samples were irradiated and gases released from the GLS were collected in separate HS vials during continuous supply of the test solutions to the photoreactor.

The photolysis system was typically conditioned for 20–30 min to ensure the UV source was at a steady-state temperature as this impacts not only the primary source intensity,[52] but also solution temperature which may have a minor effect on the GLS operation since gas solubility obeys an inverse temperature trend. It may also be noteworthy to point out that older lamps, which may have decreased spectral output despite running hotter, would compromise the reproducibility of the detected gas analytes amongst laboratories. During conditioning, DIW was continuously pumped through the system and all liquid and gas flow rates were set, stabilized and monitored before prepared samples were admitted for photolysis. Earlier experiments were conducted to pre-establish the optimal conditions for gas transfer flow rates and Ar back pressures with the aim of achieving efficient transfer and flushing of headspace vials within reasonably short time periods without excessive dilution of the released analyte gases. For this study, an Ar flow of 28 ± 1 mL min^{-1} was found effective, permitting vial flush times of typically 6 min to be used, resulting in a turn-over flushing of >15 vial volumes when real samples were processed.

The concentration ranges of TMs added to the formic and acetic acid media typically spanned reported values curated from the latest PVG literature so as to yield data/conclusions relevant to current PVG use.

Nitric acid was diluted 10-fold with DIW and used to occasionally clean the inner surfaces of the irradiated quartz lines in the PVG reactor to ensure removal of any reduced TM deposits (none visible) that may affect the photolysis processes. This was consecutively followed by several mL volumes of DIW, dilute liquid ammonia ($NH_3 \cdot H_2O$) and DIW to efficiently clean/condition the conduits.

For the analysis of H_2, a 500 μL injection (25 : 1 split ratio) of sample HS was performed and separation was obtained using an Agilent HP-PLOT Molesieve column (30 m × 0.32 mm × 25 μm, P/N 19091P-MS8) operated at constant N_2 flow rate of 1.8 mL min^{-1}. H_2 was detected at 2.4 min by TCD (temperature: 220 °C, reference flow: 18 mL min^{-1} N_2; makeup flow: 6 mL min^{-1} N_2).

For measurements of CH_4 and CO, a 750 μL injection (15 : 1 split) of sample HS drawn from the purged 10 mL glass sampling vials was performed and separation was obtained on the HP-PLOT Molesieve column operated at constant He flow rate of 1.8 mL min^{-1}. Both CH_4 and CO were detected by TCD at 7.1 and 9.9 min, respectively (temperature: 220 °C, reference flow: 18 mL min^{-1} He; makeup flow: 6 mL min^{-1} He).

For the analysis of CO_2 and light hydrocarbons (notably C_2H_6), a 250 μL injection (100 : 1 split ratio) of sample HS vial content was performed and separation was obtained on an Agilent DB-1701 column (30 m × 0.25 mm × 1 μm, P/N 122-0733) operated at constant He flow rate of 1.0 mL min^{-1} (transfer line temperature: 250 °C). The CO_2 was detected at 1.5 min by mass spectrometry in SIM mode at m/z 44, 45 and 46, whereas m/z 25, 26, 27 and 30 were monitored for the presence of other potential hydrocarbons (i.e., C_2H_6).

For expediency, the following protocol was followed: multiple analyses for each target gas were completed in all experimental systems before proceeding to measurement of the next gas of interest. Thus, CO and CH_4 were conveniently measured in each chromatographic run in all studied systems using a He carrier gas and TCD before repeating all experiments for detection of H_2 with use of a N_2 carrier gas. A full day for equilibration of the GC system was used when carrier gas was changed. Lastly, CO_2 and C_2H_6 were determined by GC-MS in SIM mode with He carrier gas, as described above.

For each test solution prepared, gas products from 3–5 replicate irradiated samples were collected in separate HS vials for analysis, reflecting products generated during steady-state photolysis of each solution. Analysis of the sample HS in a given collection vial required ∼14 min to complete for each associated GC run. This led to the need for overnight operation for periods of up to 9 h; hence the need to pre-confirm the temporal stability of the HS gas samples over a period of up to 24 h. Irrespective of TCD or MS response, analyte peak area integration was used to quantify all species based on use of proprietary Agilent MassHunter software.

Concentrations of the analyte gases produced and collected in the HS vials were based on responses from a single customized NIST traceable high purity Ar multi-gas standard containing 1000 ppm (v/v) of each gas to calibrate the TCD and MS detection systems. This was achieved by direct transfer/flushing of each headspace vial in a flow of 150 mL min^{-1} of this calibration gas for typically 3 minutes in a manner identical to that described for the samples (including dryer column as appropriate). As analytical runs may last several hours, the stability of the sampled gases and repeatability of the detection systems were verified with an earlier set of studies as being fit-for-purpose (see Results and discussion).

74 | J. Anal. At. Spectrom., 2025, 40, 70–97

This journal is © The Royal Society of Chemistry 2025

Additionally, replicate standards were prepared at the beginning of a set of experimental irradiations and two further replicates were freshly prepared at the end of such a sequence, which typically required 2–4 hours. This permitted a convenient assessment of any drift in instrument response or physical loss of sample components by diffusion/leakage during the measurement phase, as this required up to 9 hours to complete. Each HS vial was sampled only once as each needle puncture of the septum may open an avenue for potential accelerated escape of the analyte gases. Up to a 7% loss of response was incurred for both CH_4 and CO if a second HS volume was withdrawn; this manifested as a 12% loss for H_2. It was serendipitous that an earlier decision to employ a single 1000 ppm standard proved to provide a most useful reference signal that was within a factor of 2-5-fold of the range of all analyte HS gas concentrations sampled from the various PVG systems, making calibration of the detection systems over a wide concentration range unnecessary since TCD and MS are characterized as possessing several orders of magnitude linear range of operation.

For the determination of methanol, reference 5% (v/v) acetic acid solutions were irradiated at a flow rate of 2 mL min^{-1} (22 s IT) and 1.0 mL subsamples were drawn from the outlet of the flow-through photoreactor, transferred to HS vials and capped to await subsequent analysis by GC-DIB. A 20 min headspace extraction was performed while equilibrating the sample at 50 °C under magnetic stirring (500 rpm). SPME injections were manually undertaken in split mode (1 : 40) with the injector at 250 °C using He (99.999%, Messer Gases, Brazil) for sample transport and ionization at a flow rate of 1.3 mL min^{-1}. The column was subjected to a multistep thermal program starting with an initial 40 °C ramped to 50 °C at 2 °C min^{-1} and held for 1 min; a rate of 12.5 °C min^{-1} to 75 °C with hold for 2 min and finally a ramp of 30 °C min^{-1} to a final temperature of 230 °C followed by cooling. The detector was maintained at 300 °C during the total analysis time of 16 min. Instrument calibration was performed using an external calibration curve prepared in the range 1.0–30.0 mg L^{-1} methanol (5 point) spiked to ultrapure Milli-Q water and SPME extracted and analyzed in a manner identical to that for the irradiated 5% (v/v) acetic acid solutions. Non-irradiated 5% (v/v) solutions of acetic acid served as the method blank to undertake any needed corrections to the data. Peak height response was used for characterization.

Safety considerations

The full range and identity of compounds produced during PVG is unknown. Standard safety precautions should be taken during all experiments and an adequate ventilation/exhaust system should be used.

Results and discussion

Performance of sampling/detection systems

Fig. 3 shows the "long-term" temporal stability reflecting the combined contribution from collection (HS purging of vials), subsequent HS sampling of the 1000 ppm gas standard, as well as detector stability for each gas species over a period of 1–4 weeks of measurements. Individual error bars represent estimates of the

standard deviations associated with 2–4 measurements taken during evaluation of impacts of individual experimental variables on the given days (note: repeatability precision is generally too small for CH_4 and CO data and are hidden within the marker points in panel 3A). Panel 3A shows TCD detection of CH_4 and CO in He carrier (within laboratory intermediate precision = 1.5% and 1.2%, $n = 10$ and 11, respectively) over the course of a one month study. Panel 3B summarizes the trends arising during more than a week of monitoring both TCD of H_2 in N_2 carrier (intermediate precision = 2.4%, $n = 10$), and GC-MS extracted chromatograms (SIM @ m/z 44) for CO_2 in He carrier gas (intermediate precision = 6.4%, $n = 10$). These data provide assurance in both the repeatability of the performance of the sampling and detection systems during a given analytical run as well as their longer-term stability (intermediate precision) over time periods ranging from a week to more than a month of study, thereby instilling confidence in direct comparisons of data repeatedly obtained with various solutions subjected to various experimental variables.

Baseline separation of the various peaks was achieved and no extraneous interferences encountered. With the exception of specific intensities, signals arising from the 1000 ppm standards were identical to those characterizing these gases present in the effluent from the GLS derived from photolysis of the formic and acetic acids, with/without added TMs. Hydrogen was
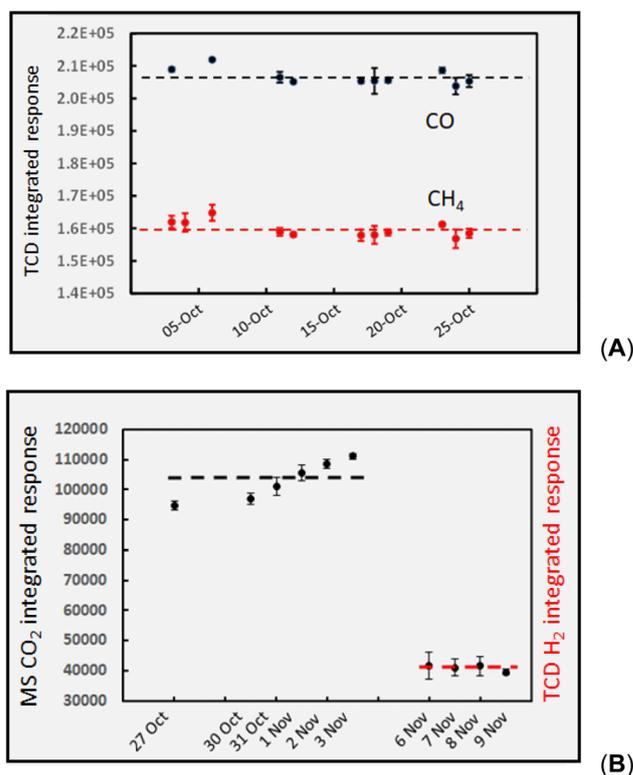
(A)

(B)

Fig. 3 "Long-term" temporal stability (within lab intermediate precision) for detection of 1000 ppm calibration standards: (A) CO (upper) with intermediate SD = 1.2%, $n = 10$ and repeatability SD = 0.81%, $n = 4$; CH_4 (lower, red) with intermediate SD 1.5%, $n = 11$ and repeatability SD = 0.76%, $n = 4$; (B) CO_2 (upper) with intermediate SD = 6.4%, $n = 10$ and repeatability SD = 2.3%, $n = 4$; H_2 (lower, red) with intermediate SD = 2.4% $n = 10$ and repeatability SD = 2.6%, $n = 3$. Ordinate displays integrated response characterizing chromatographic peaks.

This journal is © The Royal Society of Chemistry 2025

J. Anal. At. Spectrom., 2025, 40, 70–97 | 75

the only analyte that suffered measurable temporal instability, as losses from the HS vials by diffusion amounted to 5% within 4 h and 20% after 24 h. Loss rates accruing over typical 6 h data collections were assumed linear and corrected for using changes in bracketed standard intensities. Use of the NaOH dryer has no discernible impact on response for CH_4, CO, and H_2, although it efficiently removes water and acidic vapors, thereby protecting the life of the GC column.

As a consequence of the overall stability of the experimental system, integrated detector response is consistently presented as the measurement metric throughout this study rather than normalized comparisons of responses which can misrepresent data and lead to ambiguous interpretations otherwise based on stand-alone snapshots of the system. Instrument response, generated under stable measurement/sampling conditions permits the reader to comprehensively overview all data and formulate consistent trends and comparisons for each analyte of interest as experimental conditions are varied.

Part 1: PVG in the absence of added TMs

The vacuum-UV photochemistry of water is well established[53–59] and essentially summarized by the following homolysis and (to a lesser extent) charge-transfer-to-solvent reactions, respectively:
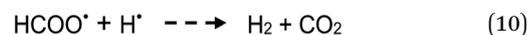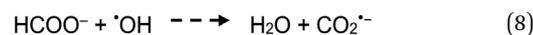
$$H_2O \xrightarrow{h\nu} H_2O^* \longrightarrow H^\bullet + {}^\bullet OH \tag{1a}$$
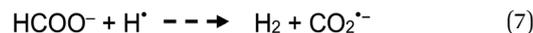
$$H_2O \xrightarrow{h\nu} H_2O^* \longrightarrow {}^\bullet OH + H^+ + e_{(aq)}^- \tag{1b}$$
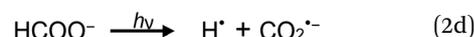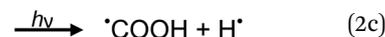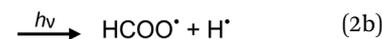
Typical of low pressure mercury discharge lamps, the intensity of 184.9 nm photons emitted by the flow-through photoreactor used in this study is likely 40-fold lower than that of the primary 253.7 nm Hg resonance line.[60] Any $H^\bullet$, ${}^\bullet OH$ and $e_{(aq)}^-$ so formed provide primary radicals that participate in the overall photolysis of dilute aqueous solutions of formic acid.[60,61] In the absence of radical scavengers (i.e., added carboxylic acids), diffusional rates of radical recombination likely inhibit significant free H_2 liberation. Zechner and Getoff[57] have demonstrated that only when formate is present at $<10^{-4}$ mol L^{-1} [i.e., $<4 \times 10^{-4}$% (v/v)] do reactions (1a) and (b) proceed, as otherwise the 185 nm incident radiation is preferentially absorbed by formate. With increasing formate concentration, reaction (7) (see below) occurs with generation of H_2. Recently, Hu et al.[62] reported photochemical hydride generation of As(III) and As(V) from an aqueous mixture of 1×10^{-3} mol L^{-1} HCOO$^-$ containing 2×10^{-3} mol L^{-1} SO$_3^{2-}$, noting ESR detection of minor amounts of $H^\bullet$, indirect evidence of $e_{(aq)}^-$, but no mention of CO$_2^{\bullet-}$. Generation of AsH$_3$ was attributed to the action of redox processes involving $H^\bullet$ and $e_{(aq)}^-$ derived from reaction (1) and photolysis of added HSO$_3^-$, suggesting that $H^\bullet$ remains an active intermediate despite the recognized high pH of this reaction medium which would lead to rapid recombination of $H^\bullet$ and ${}^\bullet OH$ radicals. Direct generation of $H^\bullet$ and $e_{(aq)}^-$ by primary photolysis of the HCOO$^-$ in accordance with reactions (2d) and (2e) (below) was not considered in this study, although at a concentration of 1×10^{-3} mol L^{-1}, absorption of 185 nm photons preferentially occurs by formate rather

than water. More recently, Jeníková et al.[63] explored the feasibility of PVG of Ru, Re and Ir from low concentrations of formic acid, noting that relatively efficient PVG processes occur during photolysis of even pure water if it is pre-saturated with CO. Thus, it was clear that efficient reduction of these elements was achieved due to available $H^\bullet$ and $e_{(aq)}^-$ radicals.
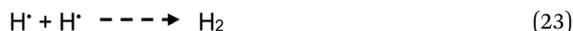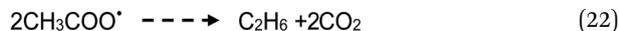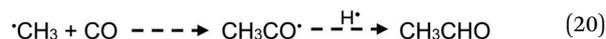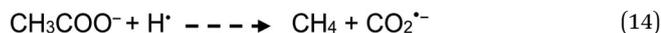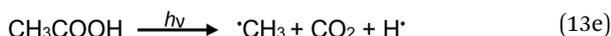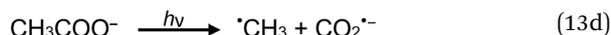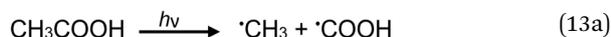
It is also expedient to review the UV-B and -C induced photolysis of formic and acetic acids, as well as briefly consider a few model LMCT reactions induced by added TMs in these acids. Reactions presented below summarize the pertinent photochemical processes that give rise to radical species which (apart from contributing to the generation of volatile metal and halogen species of analytical interest) are also the precursors to the permanent gases which are the principal subjects of this study.

Photolysis of formic acid (gas and condensed phases) has been studied for almost a century. Contrary to the belief of many organic photochemists, generation of CO occurs in addition to CO_2, albeit not as the primary reaction.[57,58,64–66] Highest relative CO/CO_2 is achieved at lower irradiation wavelengths due to rapid dissociation of the excited trans form of HCOOH to yield CO and H_2O. Several dissociation channels have also been identified by studies using 248 and 193 nm irradiation[65] (e.g., reactions (2a)–(2e)), yielding the usual powerful reducing radicals ($e_{(aq)}^-$, CO$_2^{\bullet-}$ and $H^\bullet$) which participate in subsequent thermal events (e.g., reactions (3)–(12) and denoted throughout as dashed arrows), ultimately giving rise to detectable CO, CO_2 and H_2 and characterized by overall reactions (c) and (d):

$$HCOOH \xrightarrow{h\nu} {}^\bullet CHO + {}^\bullet OH \tag{2a}$$

$$\xrightarrow{h\nu} HCOO^\bullet + H^\bullet \tag{2b}$$

$$\xrightarrow{h\nu} {}^\bullet COOH + H^\bullet \tag{2c}$$

$$HCOO^- \xrightarrow{h\nu} H^\bullet + CO_2^{\bullet-} \tag{2d}$$

$$HCOO^- \xrightarrow{h\nu} HCOO^\bullet + e_{(aq)}^- \tag{2e}$$

$${}^\bullet CHO \dashrightarrow H^\bullet + CO \tag{3}$$

$$H^\bullet + H^\bullet \dashrightarrow H_2 \tag{4}$$

$${}^\bullet CHO + {}^\bullet CHO \dashrightarrow HCHO + CO \tag{5}$$

$${}^\bullet CHO + {}^\bullet COOH \dashrightarrow HCOOH + CO \tag{6}$$

$$HCOO^- + H^\bullet \dashrightarrow H_2 + CO_2^{\bullet-} \tag{7}$$

$$HCOO^- + {}^\bullet OH \dashrightarrow H_2O + CO_2^{\bullet-} \tag{8}$$

$$2HCOO^\bullet \dashrightarrow HCOOH + CO_2 \tag{9}$$

$$HCOO^\bullet + H^\bullet \dashrightarrow H_2 + CO_2 \tag{10}$$

76 | J. Anal. At. Spectrom., 2025, **40**, 70–97

This journal is © The Royal Society of Chemistry 2025

$$\cdot COOH \dashrightarrow \cdot OH + CO \tag{11}$$

$$CO_2^{\cdot-} + HCOO^{\cdot} \dashrightarrow HCOO^- + CO_2 \tag{12}$$

$$HCOOH \xrightarrow{h\nu} CO + H_2O \quad (trans) \tag{c}$$
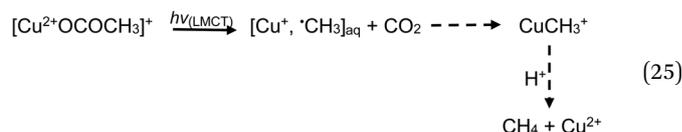
$$CO_2 + H_2 \quad (cis) \tag{d}$$

Photolysis of aqueous solutions of acetic acid have been equally long studied, wherein several routes arise and stable product yields are dependent on the degree of ionization of the acid.[67–71] Due to the greater complexity of the system, reported stable reaction products have included CH_4 and CO_2, along with H_2, methanol, formic acid and C_2H_6, summarized by generalized reaction e:

$$CH_3COOH \xrightarrow{h\nu} \cdot CH_3 + \cdot COOH \tag{13a}$$

$$CH_3COOH \xrightarrow{h\nu} CH_3CO^{\cdot} + \cdot OH \tag{13b}$$

$$CH_3COOH \xrightarrow{h\nu} CH_3COO^{\cdot} + H^{\cdot} \tag{13c}$$

$$CH_3COO^- \xrightarrow{h\nu} \cdot CH_3 + CO_2^{\cdot-} \tag{13d}$$

$$CH_3COOH \xrightarrow{h\nu} \cdot CH_3 + CO_2 + H^{\cdot} \tag{13e}$$

$$CH_3COO^- + H^{\cdot} \dashrightarrow CH_4 + CO_2^{\cdot-} \tag{14}$$

$$\cdot COOH \dashrightarrow H^{\cdot} + CO_2 \tag{15}$$

$$\cdot COOH \dashrightarrow \cdot OH + CO \tag{16}$$

$$\cdot CH_3 + H^{\cdot} \dashrightarrow CH_4 \tag{17}$$

$$\cdot CH_3 + H_2O \dashrightarrow CH_3OH + H^{\cdot} \tag{18}$$

$$\cdot CH_3 + \cdot CH_3 \dashrightarrow C_2H_6 \tag{19}$$

$$\cdot CH_3 + CO \dashrightarrow CH_3CO^{\cdot} \xrightarrow{H^{\cdot}} CH_3CHO \tag{20}$$

$$CH_3CO^{\cdot} \dashrightarrow \cdot CH_3 + CO \tag{21}$$

$$2CH_3COO^{\cdot} \dashrightarrow C_2H_6 + 2CO_2 \tag{22}$$

$$H^{\cdot} + H^{\cdot} \dashrightarrow H_2 \tag{23}$$

$$CH_3COOH \dashrightarrow CH_4 + CO_2 \text{ (minor: } CO, H_2, C_2H_6) \tag{e}$$
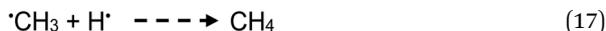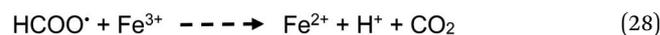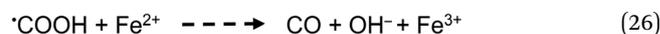
Note that no consideration has been given to the existence of stable dimers of both carboxylic acids in aqueous solutions[72] which may initiate their own sets of radical based reactions.[67]

Addition of TMs to either acid results in the formation of TM-carboxylate complexes, which may exhibit not only d–d transitions of the metal center, but also photochemical

(LMTC) reactions, as noted earlier. Typical examples are presented below for the case of iron and copper,[42,44,60] wherein LMCT processes take place at significantly longer wavelengths outside the UV-C spectral window needed for homolysis of water and oxidation of formic/acetic acids. Thus, advantage may be taken of the intense UV-B spectral region emitted from low pressure mercury discharge sources, enhancing generation efficiencies of $H^{\cdot}$ and $\cdot CH_3$ radicals as well as production of CO_2:

$$[Fe^{3+}HCO_2^-]^{2+} \xrightarrow{h\nu_{(LMCT)}} Fe^{2+} + HCO_2^{\cdot} \dashrightarrow H^{\cdot} + CO_2 \tag{24}$$

$$[Cu^{2+}OCOCH_3]^+ \xrightarrow{h\nu_{(LMCT)}} [Cu^+, \cdot CH_3]_{aq} + CO_2 \dashrightarrow CuCH_3^+ \xrightarrow[\quad]{H^+} CH_4 + Cu^{2+} \tag{25}$$

Apart from the above processes potentially directly influencing the sources and concentrations of radicals giving rise to CO, CO_2, H_2 and CH_4 in TM-doped PVG systems, the added TMs may also be involved in secondary thermal radical catalytic redox reactions which further influence the relative concentrations of some gases, including, for example:[50,73,74]

$$\cdot COOH + Fe^{2+} \dashrightarrow CO + OH^- + Fe^{3+} \tag{26}$$

$$HCOO^{\cdot} + Fe^{2+} \dashrightarrow HCOO^- + Fe^{3+} \tag{27}$$

$$HCOO^{\cdot} + Fe^{3+} \dashrightarrow Fe^{2+} + H^+ + CO_2 \tag{28}$$

$$TM^0 + n\,\cdot CH_3 \dashrightarrow TM(CH_3)_n \tag{29}$$

The extent to which added TMs perturb generation of radical intermediates should thus be reflected in relative changes in HS gas composition between irradiated TM-spiked and -unspiked PVG media. As noted earlier, this provides a new tool for probing mechanistic aspects of PVG which should not only complement results from earlier ESR studies, but also provide a broader profile, as H_2 and CO become useful probes in addition to the usual $\cdot CH_3$, $\cdot OH$ and $CO_2^{\cdot-}$ radical species reported with ESR, which primarily serve as indicators of the reductive potential of irradiated media.

Although the principal objective of this study was to utilize these results to establish comparative rates of production of the various gases as a function of experimental variables, use of Henry's Law and the known dilution factor arising from the GLS gas transfer process suggest that, at the least, semiquantitative concentrations of CO, CO_2, CH_4 and H_2 may also be estimated. The solubility of CO_2 in water presents the worst case scenario as its dissolution is the most favorable, as evident from its Henry's Law constant, typically an order of magnitude greater than that for the other gases due to its reaction to form H_2CO_3. All photolysis media used in this study have a pH < 3, providing favorable conditions for decreased solubility of CO_2 as the reaction to form carbonic acid is suppressed. Thus, complete

This journal is © The Royal Society of Chemistry 2025

J. Anal. At. Spectrom., 2025, **40**, 70–97 | 77

release of even CO_2 can be expected.[75,76] Irrespective, relative changes in the targeted gas concentrations in the TM-unspiked formic and acetic acid systems can be directly compared to those generated in the presence of added TMs to provide insight into the relevance of the LMCT model in accounting for changes in PVG efficiencies because all experimental variables are carefully replicated and any perturbation reflects only the impact of the added TM.

To appreciate the effects of the presence of added TMs, it is instructive to first consider the baseline or "endogenous" concentrations of the gases of interest that are photolytically generated in their absence and their response to changes in experimental variables typically undertaken during optimization of PVG efficiency, *i.e.*, impact of the concentrations of the formic and acetic acids, sample irradiation time and use of mixtures of these acids.

To ensure the relevance of these experiments, a comprehensive examination of the PVG literature published since 2015 based on available use of thin-film flow through photoreactors was used to identify relevant concentration ranges of formic and acetic acids for study, typical concentrations of added TMs to be investigated as well as irradiation times. As such, observed trends can be correlated with those typical of published analytical PVG results wherein response from synthesis of targeted volatile metal species has been examined under similar experimental conditions.

Contamination introduced by the sampling process was validated by running DIW blanks through the fully powered PVG system. No response was detected from CO, CH_4 and H_2 while that for CO_2 was consistently in the range 5–10% of the typical concentrations evolved from irradiated samples of 5% (v/v) formic and acetic acids, corresponding to 285 ± 50 ppm CO_2 in the collected sample HS (averaged over 7 days of testing). Its source was never investigated in detail and although the DIW system was fitted with a UV oxidation unit, it is possible that it was inefficient and the "blank" CO_2 measurement corresponded to oxidation of residual organic contaminants in the water, as the level appears too high to be the result of dissolution of atmospheric CO_2 (nominally 420 ppm) over such short exposure times.

Hydrogen production *via* photolysis of water

Photolysis of pure water was investigated for evolution of H_2, as this is the only gaseous species of interest potentially produced. In connection with the results of Zechner and Getoff,[57] the impact of dilute solutions of formic acid serving as an H˙ radical scavenger (*via* reaction (7)) was also examined.

Replicate GC-TCD analyses of HS H_2 content derived from the photolysis of DIW revealed no quantifiable response above baseline noise. Homolysis reaction (1a) is likely rapidly reversible as initially a cage complex must be generated permitting subsequent diffusion limited recombination of the H˙ and ˙OH species. Interestingly, however, is that photolysis of a very dilute solution of 0.004% (v/v) formic acid generated measurable quantities of H_2, far in excess of that expected based on the amounts released from subsequently explored solutions of

1000-fold higher concentrations. Thus, while photolysis of 5% HCOOH at a flow rate of 2 mL min⁻¹ typically provided 380 ± 40 ppm H_2 in the HS (see Table 1), that from 0.004% (v/v) formic acid produced 110 ± 10 ppm H_2. The disproportionate synthesis of H_2 in this very dilute medium suggests that either homolysis of water is efficient and reaction (7) serves to trap the generated H˙ before extensive radical recombination can occur to yield H_2 (as with commonly used ESR spin trapping reagents), or that the penetration depth of 185 nm photons is enhanced by at least 100-fold as the HCOOH concentration is reduced from 5 to 0.004%. Irrespective, recent studies by Musil *et al.*[63] which reported on the successful generation of several metal carbonyls during photolysis of only deionized water that was pre-saturated with CO provides evidence for the efficacy of reactions (1a) and (b) liberating reducing radicals that create free atoms of metals which subsequently coordinate with available CO to yield their volatile molecular carbonyls. Moreover, sufficient liberation of H˙ is evident in 0.004% formic acid to permit synthesis of volatile species of hydrides, such as Se.[63]

Gas production *via* photolysis of formic acid

A formic acid medium is the simplest to consider first, as only H_2, CO and CO_2 are of interest. All data are reported based on the volumetric concentrations of the carboxylic acids (rather than molarity) as this is the most common means of preparing such experimental PVG media and reporting their impact in the analytical literature. Note also that, unless specifically calculated, all concentration data reported for the various gases are uncorrected for the dilution effect imposed by the 28 mL min⁻¹ flow of Ar transport gas used to flush the products from the GLS to the HS sample vials.

Generation of CO. Fig. 4A illustrates the effect of concentration of formic acid on production of CO arising from the photolysis of solutions delivered at 2.0 mL min⁻¹ to the photoreactor (corresponding to an irradiation time of IT = 22 s). An uncorrected average concentration over the duration of all experiments of 3760 ± 220 ppm (intermediate SD, $n = 11$) was determined in the HS samples produced by photolysis of a 5% (v/v) solution, which will henceforth be arbitrarily used as the reference or benchmark for comparisons throughout this study using both formic and acetic acids.

Several points merit discussion of these data. It is noteworthy that the non-linear asymptotic characteristic of this curve mirrors those illustrating the impact of carboxylic acid concentration (in both HCOOH and CH_3COOH systems) on analytical PVG yields for numerous elements.[16,22,26,28,30,31,77–84] The downward curvature is frequently attributed to the decreased depth of penetration of the UV-C radiation into the bulk of the sample as the acid concentration is increased, thereby lowering the effective photon flux to the bulk or core of the flowing solution. In the case of formic acid (and similarly acetic), its significant molar absorption coefficient (34.9 M^{-1} cm^{-1} at 185 nm)[85] results in a penetration depth (depth at which attenuation of source intensity of 185 nm radiation is reduced to 10%) of 240 μm into a 5% (v/v) medium (similar results hold for acetic acid as well). Unless turbulent

mixing is achieved in the 2 mm diameter sample conduit, its central core receives significantly fewer photons; photolysis efficiency is expected to correspondingly diminish with increased [HCOOH].

Additionally, it has been reported that the rate of photolysis of HCOOH is dependent on its degree of ionization.[59,70] Being a weak acid, increased HCOOH concentration corresponds to a decreased relative [$HCOO^-$] and a potentially concurrent quadratic relationship between [HCOOH] and CO yield. Adams and Hart[60] concluded that UV photolysis of HCOOH resulted in production of CO via reactions 3, 5, 6 and 11, involving $^\bullet CHO$ and $^\bullet COOH$ intermediates. Unless the [HCOOH] is $<10^{-4}$ mol L^{-1} [i.e., <0.001% (v/v)], the contribution of subsequent thermal reactions involving $H^\bullet$ and $^\bullet OH$ (arising from homolysis of water, reaction (1)) with $HCOO^-$ (reactions (7) and (8)) to generate H_2 and $CO_2^{\bullet-}$ are insignificant due to the molar absorption coefficient for H_2O being 10^3-fold smaller than that of $HCOO^-$ at 185 nm.[57,85]

Based on its low solubility, Henry's law predicts a negligible concentration of CO remains dissolved in the irradiated solution; furthermore, the thin-film geometry of the GLS serves to efficiently release it to the counter-current flow of 28 mL min^{-1} Ar. Reactions (3), (5), (6) and (11) serve to generate CO, but irrespective of the mechanism, reaction (c) shows that a 5% (v/v, $\sim$1.18 mol L^{-1}) solution of HCOOH irradiated at a flow rate of 2 mL min^{-1} will quantitatively generate 2.4 mmol min^{-1} CO, equivalent to 53 mL min^{-1}. When diluted in a flow of 28 mL min^{-1} Ar, the sampled HS mixture should contain 6.5×10^5 ppm CO. Based on the average determined HS CO concentration of 3760 ± 220 ppm (cf. Table 1), an apparent oxidation (photolysis) efficiency of only 0.6% is revealed. Considering the possible need for an ionized precursor[59] and the relatively low flux of source photons at 185 nm, this estimate is perhaps not surprising. Due to the low degree of ionization (α) of HCOOH (i.e., $\alpha = 1.2\%$ at 1.18 mol L^{-1}; $K_a = 1.78 \times 10^{-4}$), a 5-fold increase in [HCOOH] yields a 2.2-fold increase in [$HCOO^-$] and can quantitatively account for the experimentally observed rise in CO as the formic acid concentration is augmented from 2 to 10% (v/v), evident in Fig. 4A. This suggests that penetration of UV-C photons may not present such a significant impediment to photolysis in this flow-through reactor in this range of formic acid concentration. Although not shown in Fig. 4A, decreasing the sample flow rate to 1 mL min^{-1} (thereby increasing the irradiation time to 43 s), resulted in a 1.5-fold increase in CO from a 2% (v/v) HCOOH medium to yield a 3520 ± 190 ppm (repeatability SD: $n = 3$) CO headspace concentration. Note that when corrected for the rate of delivery of product at the exit of the GLS, this would result in an equivalent 3-fold increase in yield for a doubling of the irradiation time. Unaccounted for losses of primary generated CO via such processes as the water gas shift reaction are unlikely due to both the low temperature and low H_2 partial pressure, as well as the absence of a catalyst.

Generation of H_2. Fig. 4B shows the effect of [HCOOH] on H_2 synthesis. As with CO, a non-linear dependence is evident. Adams and Hart[60] suggested that although there is a dependence of both H_2 and CO on photolytic source intensity, the primary generated $^\bullet CHO$ (reaction (2a)) is subsequently involved in one or more radical–radical competitive (thermal) reactions (i.e., reactions (3), (5) and (6)).

An estimate of overall photolysis efficiency with respect to H_2 production may be made based on reaction d. Using data averaged from all experiments based on a 22 s photolysis of 5% HCOOH (sample flow rate of 2 mL min; $H_2 = 380 \pm 40$ ppm, intermediate SD, $n = 7$, cf. Table 1) in the collected HS samples and calculations similar to those outlined above for CO, suggests an oxidation efficiency of 0.05%, an order of magnitude inferior to that based on CO data. It is clear that these reactions are not directly coupled (reactions (c) and (d)) and details of the quantum yields, excitation/dissociation and kinetics of processes leading to CO and H_2 generation would have to be taken into account to arrive at more accurate
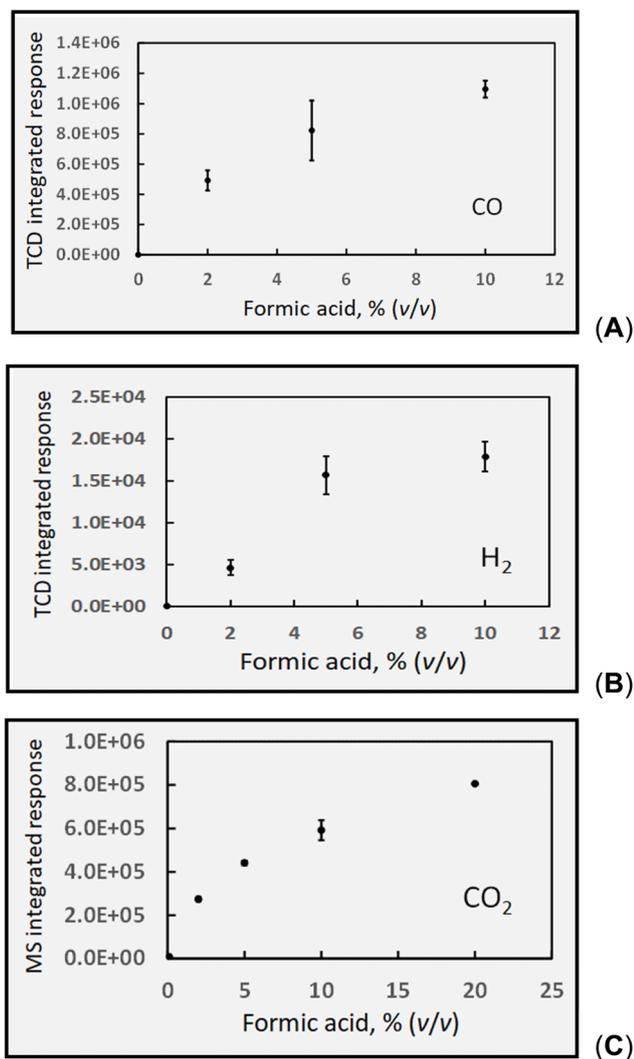
Fig. 4 Effect of formic acid concentration on analyte gas response (production) at 2 mL min^{-1} solution flow rate (IT = 22 s). (A) CO production, uncorrected HS [CO] = 3810 ± 930 ppm (repeatability SD, $n = 2$) at 5% (v/v) formic acid; (B) H_2 response (production), uncorrected HS [H_2] = 400 ± 60 ppm (repeatability SD, $n = 3$) at 5% (v/v) formic acid; (C) CO_2 response (production), uncorrected HS [CO_2] = 4290 ± 100 ppm (repeatability SD, $n = 5$) at 5% formic acid. Ordinate displays integrated response characterizing chromatographic peaks.

estimates of reaction yields. Nevertheless, together they consistently suggest a low overall oxidation efficiency. Unless a complete analysis of all reaction products can be accomplished, differentiation of the chemical (thermal) interactions of the various radicals cannot be discerned.

Similar to CO (and not shown in Fig. 4B), H_2 generation from 5% (v/v) HCOOH at a 1 mL min^{-1} sample flow rate (irradiation time of 43 s) was enhanced 1.9-fold to yield 720 ± 75 ppm (repeatability SD, $n = 3$) headspace concentration. This occurs despite the 2-fold reduction in the rate of delivery of H_2 to the GLS, indicating that a doubling of irradiation time enhanced efficiency of H_2 production by 4-fold. Similar correlations are evident in the analytical PVG literature wherein response from targeted (UV-stable) metal analytes frequently increases with irradiation time but typically not as dramatically as for these gases, indicating a potential loss mechanism which may be putatively assigned as a concurrent competitive UV photolytic decomposition of the (unstable) metal analyte species.

Generation of CO_2. The most abundant stable gaseous product arising from photolysis of HCOOH is CO_2. Based on similar calculations invoked for CO and H_2, and as a result of the suppressed solubility of CO_2 in the low pH medium (less than 5% of the HS CO_2 remains dissolved in the GLS waste), a further independent estimate of the degree of photolytic oxidation of HCOOH can be undertaken (from Table 1, based on reaction d) to yield a value of 0.7%, in agreement with that derived from CO data. Fig. 4C shows the impact of increasing [HCOOH] on CO_2 yield. Although reactions such as 9, 10 and 12 may directly generate CO_2, $CO_2^{\cdot-}$ is also abundant in formate media (reactions (2d), (7) and (8)) and its oxidation (through dissolved O_2) can give rise to CO_2.[86] Note that generation of CO_2 is detected in the absence of added HCOOH (or acetic acid) and likely reflects oxidation of possible residual dissolved organic impurities as well as any dissolved CO_2 arising from atmospheric ingress into the DIW medium supporting the PVG reactions, yielding an equivalent 285 ± 50 ppm (repeatability SD, $n = 7$) HS concentration. As the irradiation time was doubled (from 22 to 43 s) by decreasing the solution flow rate from 2 to 1 mL min^{-1}, the headspace CO_2 concentration arising from photolysis of 5% formic acid increased from 4290 ± 100 ppm (repeatability SD, $n = 5$) to 6400 ± 260 ppm (repeatability SD, $n = 5$), a 1.5-fold increase (3-fold when corrected for actual flux).

Over a measurement period of 10 days, comprising 9 discrete experiments, an average (blank corrected) concentration of 4440 ± 310 ppm CO_2 (intermediate SD, $n = 13$; cf. Table 1) was determined in the sample HS comprising GLS effluent from photolysis of 5% (v/v) formic acid at 2 mL min^{-1} (IT = 22 s).

Gas production *via* photolysis of acetic acid

The majority of published literature concludes that CO_2 and CH_4 are the principle gaseous products of photolysis of acetic acid. However, other reported by-products have included C_2H_4, CH_3OH and acetaldehyde, likely arising from secondary recombination reactions consuming $\cdot CH_3$ radicals. Several thermal radical reactions also lead to production of CO

(reactions (16) and (21)) and H_2 (reaction (23)), although they are expected to be of low yield. As is the case with HCOOH, at the concentration levels of interest to this study, direct photolysis of CH_3COOH and CH_3COO^- likely dominate reactions as compared to those initiated by $H^{\cdot}$ and $\cdot OH$ homolysis processes arising from eqn (1a) and (b) due to their higher molar absorptivity compared to that for DIW. Note that the equivalent molarity of the photolyzed solutions of formic and acetic differ by a factor of 1.4, reflecting the lower concentration of the neat acetic acid; this is expected to result in lower HS concentrations of the measured gases common to the two systems.

Generation of CO_2. As evident in Fig. 5A, significantly less (2-fold, even accounting for molarity difference) CO_2 is generated in the acetic acid system compared to the formic acid system (cf. Fig. 4C). A mean HS concentration of 1700 ± 130 ppm (intermediate SD, $n = 9$; cf. Table 1) reflecting data obtained over the duration of the study was determined for photolysis of 5% (v/v) acetic acid. An asymptotic-like dependence on acid concentration is also evident for production of this gas, suggesting an impact of photon penetration depth on the oxidation efficiency. The CO_2 yield can be increased by 1.7-fold when irradiation is conducted at a solution flow rate of 1 mL min^{-1} (IT = 43 s to yield a HS [CO_2] = 2960 ± 130 ppm), suggesting that the actual process is enhanced 3.4-fold after accounting for the reduced analyte flux to the ICP which occurs at 1 mL min^{-1} sample delivery rate. Considering the difference in molarity of the 5% solutions of formic and acetic acids (1.18 vs. 0.87 M), formic acid still generates/releases 1.9-fold greater concentrations of CO_2 than acetic acid. As noted earlier, if the rates of photolysis of formic and acetic acids are related to their degrees of ionization (α),[59] the calculated values of 1.2% and 0.46% for formic and acetic acid, respectively, may simply account for the higher relative yield of CO_2 generated by photolysis of formic acid (pH of the respective 5% (v/v) formic and acetic acid solutions is 1.85 and 2.40). Based on the average production of 1700 ppm CO_2 in 5% acetic acid (cf. Table 1) and the 1 : 1 stoichiometry for oxidation of CH_3COOH summarized by equation e, an efficiency of 0.5% can be estimated, somewhat higher than that calculated below from data based on production of CH_4 in this system, but similar to that calculated for the formic acid system.

Generation of CO. No direct photolysis route arises for generation of CO from acetic acid. However, a possible trace concentration of HCOOH as an impurity present at 0.05% (v/v) could fully account for the detection of 14 ± 4 ppm (repeatability SD, $n = 9$, cf. Table 1) CO measured over the course of one month of study of the sampled HS gas arising from photolysis of 5% (v/v) acetic acid. As noted by Mittal et al.,[70] HCOOH has also been reported as a product of photolysis of aqueous acetic acid. Although the mechanism was not disclosed, earlier work by Burton[67] suggested a potential secondary thermal route to CO formation as shown by reaction (16). Scavenging of CO at higher concentrations of acetic acid due to increasingly larger concentrations of $\cdot CH_3$ to generate methanol, acetaldehyde (and possibly diacetyl)[40] in accordance with reactions (18) and (20) cannot be ruled out. Acetaldehyde was not investigated in this system, but directed measurements of methanol
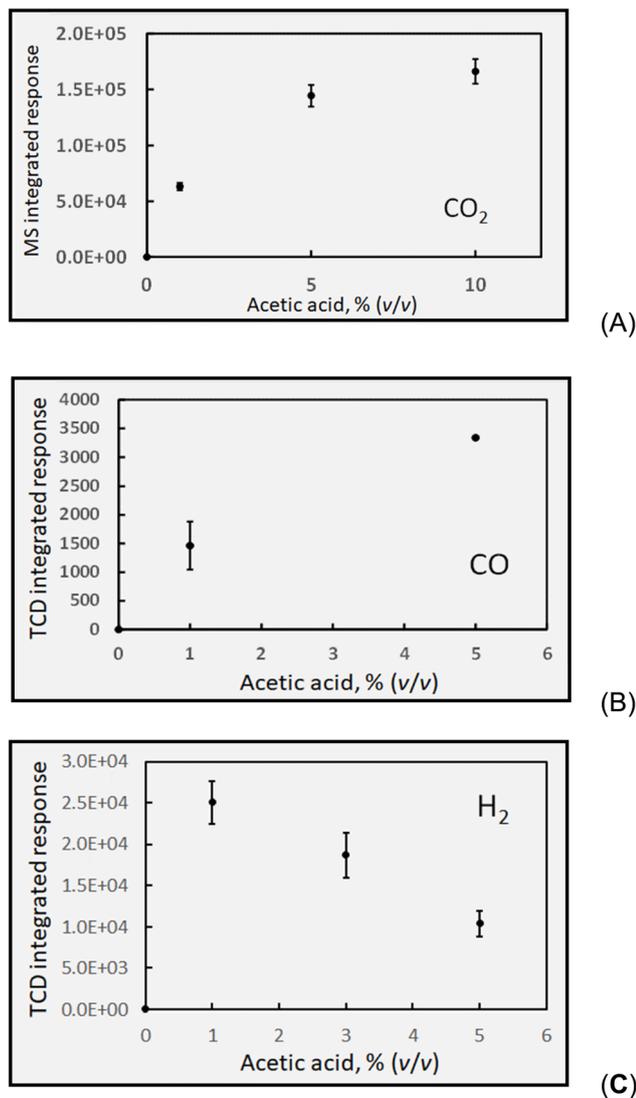
80 | *J. Anal. At. Spectrom.*, 2025, **40**, 70–97

This journal is © The Royal Society of Chemistry 2025

Fig. 5 Effect of acetic acid concentration on analyte gas response (generation) at 2 mL min^{-1} solution flow rate (IT = 22 s). (A) CO_2 production, uncorrected HS [CO_2] = 1730 ± 30 ppm (repeatability SD, n = 4) at 5% (v/v) acetic acid. (B) CO production, uncorrected HS [CO] = 14 ± 4 ppm (repeatability SD, n = 9) at 5% (v/v) acetic acid. (C) H_2 production, uncorrected HS [H_2] = 290 ± 40 ppm (repeatability SD, n = 3) at 5% (v/v) acetic acid. Ordinate displays integrated response characterizing chromatographic peaks.

production arising from irradiation of 5% (v/v) solutions of acetic acid were undertaken. As noted earlier, due to its miscibility in water, a separate extraction and analysis methodology was applied; results are discussed in the section below relating to CH_4 generation. Such low concentrations of CO are not expected to support synthesis of organometallic carbonyl species; indeed, generation of TM carbonyls from acetic acid media is not significant.

Generation of H_2. As noted earlier, homolysis of water can be discounted as a source of H_2 at the concentrations of acetic acid studied here (>0.17 mol L^{-1}) due to its poorly competitive molar absorption coefficient for UV-C radiation, which is primarily attenuated by the carboxylic acid. Interestingly, the presence of

a small HCOOH impurity implied to account for the production of CO in this medium may also contribute to generation of small amounts of H_2. Nevertheless, reactions (13c) and (13e) do provide a primary route to the photolytic production of H_2 (via reaction (23)) whereas reactions 15 and 18 suggest additional thermal routes; in particular, the reaction of $^{\bullet}CH_3$ with H_2O provides a likely scenario. In any case, the generally reported overall photo-oxidation reaction (e) does not suggest it as a typically significant product, likely as it refers primarily to gas phase photolysis of anhydrous acetic acid. It is thus surprising/significant to see both the magnitude of the amount of H_2 generated, as well as the negative impact of increasing concentrations of acetic acid on its yield (approximating conditions closer to the anhydrous reagent), which may be accounted for by the presence of several competitive sinks (reactions (14) and (17)), not the least of which is formation of CH_4. Photolysis of solutions of 3% acetic acid at 1 mL min^{-1} increases H_2 concentration in the HS by 1.5-fold (to 640 ± 60 ppm) compared to 2 mL min^{-1} production yields, implying an overall 3-fold increase in the extent of synthesis.

Generation of CH_4. Fig. 6A shows the relative production of CH_4 arising from the photogeneration of $^{\bullet}CH_3$. A trend similar to that for general production of gases in the HCOOH system is evident and may point to a limiting rate of generation due to the impact of depth of penetration of the UV-C photons into the irradiated medium since the molar absorption coefficient at higher acetic acid concentrations is similar to that for HCOOH.

The methyl radical is quite reactive and can function as both an oxidant and reductant, which may alter its perceived stoichiometry of net production as presented by overall reaction e. During analytical PVG of the halogens, its oxidizing character is evident in the capture of nucleophilic X$^{\bullet}$ to yield CH_3X. By contrast, it also serves as a strong reductant towards water, producing methanol, as illustrated by reaction (18), which will become more significant at higher concentrations of acetic acid. The general shape of the response curve is similar to that obtained with analytical PVG optimization experiments for elements synthesized as methylated species from an acetic acid medium.

Over the course of one month, comprising 7 discrete experiments, an average concentration of 1180 ± 150 ppm (intermediate SD, n = 14; cf. Table 1) CH_4 was determined in the sample HS derived from the GLS effluent from photolysed 5% (v/v) acetic acid solutions. Based on this, and neglecting any potential losses of $^{\bullet}CH_3$ precursor via other reactions, an estimate of the overall oxidation efficiency of CH_3COOH at a flow rate of 2 mL min^{-1} in accordance with reaction (e) and calculated in the same manner as described earlier for CO in the formic acid system, yields a photolysis efficiency of 0.2% [note that a 5% (v/v) solution of CH_3COOH corresponds to an 0.85 mol L^{-1} solution (and a smaller α of 0.4%)].

Loss of $^{\bullet}CH_3$ via reaction (18) can occur to yield methanol. To estimate the impact of this potential sink, the concentration of methanol produced in irradiated 5% acetic acid was determined by SPME-GC-DIB to be 3.7 ± 0.3 mg L^{-1} (reproducibility SD, n = 3). Assuming no methanol formed in the irradiated samples was lost through evaporation during the short
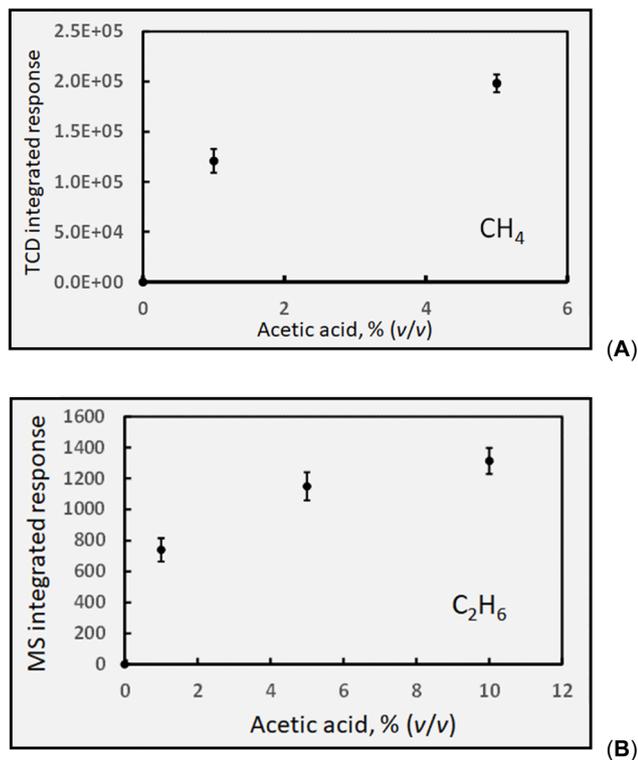
This journal is © The Royal Society of Chemistry 2025

J. Anal. At. Spectrom., 2025, **40**, 70–97 | 81

Fig. 6 Effect of acetic acid concentration on response (generation) of: (A) HS CH_4 at 2 mL min^{-1} solution flow rate (IT = 22 s). Uncorrected HS $[CH_4]$ = 1250 ± 60 ppm (repeatability SD, n = 3) for 5% (v/v) CH_3-COOH. (B) HS C_2H_6 response (generation) at 2 mL min^{-1} solution flow rate. Uncorrected HS $[C_2H_6]$ generated in 5% acetic acid estimated as ~30 ppm (error bars show repeatability SD: n = 3). Ordinate displays integrated response characterizing chromatographic peaks.

collection phase, and that all methanol originated from photogenerated $^{\bullet}CH_3$ reacting with water in accordance with reaction (18), the yield can be calculated to be 1.7×10^{-7} mol mL^{-1}, equivalent to a synthesis efficiency of 0.014%. This may be contrasted to the earlier estimate of 0.2% generation efficiency $^{\bullet}CH_3$ derived from the measured yield of CH_4 in this medium (Table 1, characterizing reaction (e)) and to the conclusion that losses of CH_4 through formation of methanol amount to less than 10%.

Generation of C_2H_6. Ethane is a thermal by-product of the photolysis of acetic acid arising from dimerization of $^{\bullet}CH_3$ radicals (reaction (19)). It is not produced during photolysis of formic acid, as expected, and is detected concurrently with CO_2 by examination of GC-MS SIM response at m/z = 30. Its' general dependence on $[CH_3COOH]$, shown in Fig. 6B, mirrors that of CH_4. A standard for ethane was not available for instrument calibration, but based on a study by Hamid *et al.*,[71] wherein the ratio of $C_2H_6 : H_2$ reportedly produced during photolysis of aqueous solutions of acetic acid was 1 : 17, an estimated concentration of ethane in the GLS effluent during photolysis of 5% (v/v) acetic acid yields 16 ppm. Similarly, Mozia *et al.*[87] reported a $C_2H_6 : CH_4$ ratio of 0.03 for the photo-Kolbe oxidation of acetic acid solution in the presence of decorated TiO_2, suggesting the concentration of ethane could be in the range of

30 ppm herein. It is clear that this species is characterized by low generation efficiency, despite the likely beneficial effects arising from the presence of photocatalysts in such media.[87]

Table 1 presents a summary of the HS concentrations of stable gas species generated during the photolysis of 5% (v/v) reference concentrations of both formic and acetic acids irradiated for 22 s in the flow-through photoreactor (solution flow = 2 mL min^{-1}). As has been noted throughout, the detected HS concentrations are *not* corrected for volumetric dilution introduced by the carrier gas flow of 28 ± 1 mL min^{-1} Ar, but may be corrected as attempted for some earlier examples used for estimation of oxidation efficiency of the acids based on overall reaction stoichiometries (eqn (13a)–(13e)). Moreover, with a 1.4-fold higher molarity of formic acid, all other factors aside (relative α, solubility), relative concentrations of their one common gas, CO_2, should theoretically be 40% higher in formic acid. Details of interaction of the source intensity and wavelength with the different acids need to be taken into account along with all subsequent thermal reactions involving the photolytically generated precursor radicals in order to present a clearer picture, but this is not possible within the scope of this study.

Table 1 Summary of averaged HS gases from 5% (v/v) media, ppm[a]

	CO	H_2	CH_4	CO_2
Formic	3760 ± 220(11)	380 ± 40(7)	—	4440 ± 310(13)
Acetic	14 ± 4(9)	240 ± 35(6)	1180 ± 150(14)	1700 ± 130(9)

[a] Intermediate precision expressed as standard deviation over duration of study encompassing (n) measurements. Note: data are HS concentrations and thus uncorrected for dilution arising from GLS Ar carrier gas flow of 28 mL min^{-1}.

Photolysis of mixed acid media

A number of analytical PVG studies have reported enhanced synthesis yields of targeted metal species when using mixtures of formic and acetic acids.[20,21,28,88] Hou and colleagues[20] utilized spin-trapping ESR detection techniques to present evidence that more $CO_2^{\bullet-}$ was generated in a mixed formic/acetic acid medium than in their individual solutions of the same concentration. In the case of Te and other semi-metals that give rise to methylated PVG analogs, it is possible that differences in the molar absorption coefficients for formic acid at lower wavelengths increase generation of $CO_2^{\bullet-}$ to provide a more reducing medium for efficient metal ion reduction, although it is $^{\bullet}CH_3$ available from acetic acid that drives final product formation. Additionally, CO can rapidly scavenge $^{\bullet}OH$ to provide a yet more favorable population of $H^{\bullet}$ reducing radicals:[89]

$$^{\bullet}OH + CO \longrightarrow CO_2 + H^{\bullet} \qquad (30)$$

It is noteworthy, however, that use of mixtures of carboxylic acids does not universally endow analytical PVG with positive impacts. Musil and colleagues reported that PVG of both Mo^{30} and W^{16} provided superior generation efficiency of their metal carbonyls (as well as for those of Fe, Ni and Co) from solely formic

82 | *J. Anal. At. Spectrom.*, 2025, **40**, 70–97

This journal is © The Royal Society of Chemistry 2025

acid as compared to a formic/acetic mixture. For transition metals which form primarily stable carbonyl species, this negative impact can be ascribed to the consumption of CO by $\cdot CH_3$ radicals to yield $\cdot CH_3CO$ and subsequently $CH_3COCOCH_3$, CH_3CHO and CH_3-$COOH$.[8] As an example, the relative effects of a mixed acid medium comprising 5% (v/v) formic and 5% acetic (v/v) on production of CO and CH_4 headspace gases are compared to those of their individual solutions in Fig. 7.

Responses (repeatability SD, $n = 3$) to production of both CO in formic acid and CH_4 in acetic acid (5% (v/v)) are in statistical agreement with those shown earlier in Fig. 4A and 6A respectively, illustrating the stability of the systems throughout this study. Importantly, addition of acetic acid to formic acid produces a significant depletion of CO in this medium whereas addition of formic acid to acetic acid results in a more deleterious effect on the generation of CH_4 in the mixture. Both effects may be attributed to reaction 31.[40]

$$CO + \cdot CH_3 \longrightarrow CH_3CO \cdot \longrightarrow CH_3COCOCH_3/CH_3CHO/CH_3COOH \quad (31)$$
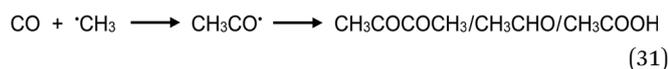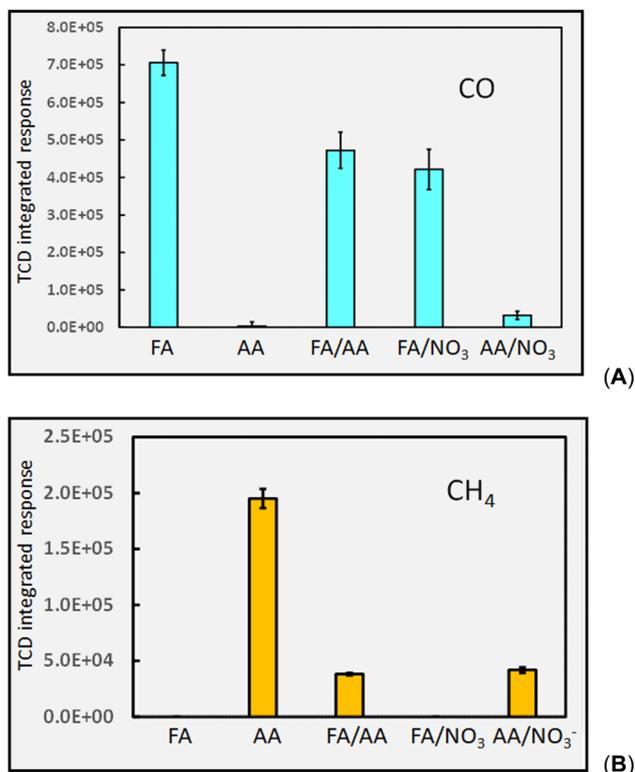
Providing a well-founded fundamental basis for these practical observations.
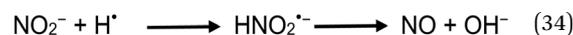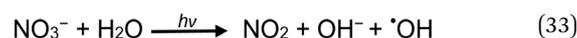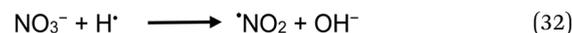
(A)

(B)

Fig. 7 Impact of PVG medium composition on HS response from: (A) CO and (B) CH_4. FA = 5% formic acid (v/v); AA = 5% acetic acid (v/v); FA/AA = mixture of 5% (v/v) each acid; FA/NO_3^- = 5% (v/v) formic acid containing 10 mM NO_3^-; AA/NO_3^- = 5% acetic acid (v/v) containing 10 mM NO_3^-. 2 mL min^{-1} solution irradiation (IT = 22 s). Repeatability SD, $n = 3$. Ordinate displays integrated response characterizing chromatographic peaks.

Impact of NO_3^- as a common interference on gas production

Fig. 7 also illustrates the significant effect addition of 10 mM NO_3^- (present as KNO_3) into the generation medium has on decreasing CO and CH_4 production by an order of magnitude, far more impactful that the effect of any other experimental variable examined. Dissolved O_2, NO_3^-, NO_2^- and Cl^- are recognized quenchers of radical based reactions due to their affinity for hydrated electrons and hydrogen atoms.[90–95]

$$NO_3^- + H\cdot \longrightarrow \cdot NO_2 + OH^- \quad (32)$$

$$NO_3^- + H_2O \xrightarrow{h\nu} NO_2 + OH^- + \cdot OH \quad (33)$$

$$NO_2^- + H\cdot \longrightarrow HNO_2^{\cdot-} \longrightarrow NO + OH^- \quad (34)$$

$$O_2 + e_{(aq)}^- \longrightarrow O_2^{\cdot-} \quad (35)$$

Suppression of CH_4 generation in acetic acid containing added NO_3^- is also a consequence of the scavenging of $H\cdot$. Although all analytical PVG systems suffer to some extent from the presence of oxidants such as nitrate and nitrite (a product of photoreduction of NO_3^-),[1] PVG yield of Se(IV) from formic and acetic acid media presents a particularly severe example.[96,97]

Fig. 8 quantifies the very severe interference (i.e., almost complete suppression) that the presence of 10 mM NO_3^- has on H_2 production from 5% solutions of acetic and formic acids. Its seemingly more dramatic impact on the formic acid system may be a consequence of the more complex environment present in acetic acid. The consequences of thermal reactions involving radicals other than those of $H\cdot$ (as illustrated in reactions (32) and (34)) with the photolysis products of nitrate are unknown. A gas profile of the photolysis products of nitrate would likely shed more light on what is occurring in these systems to provide for a more holistic picture of events.

It is interesting that PVG of Se(IV) from formic acid generates a mixture of both SeH_2 (~70%) and SeCO (~30%). However, in the presence of 10 mM $NaNO_3$, formation of SeH_2 is completely suppressed, with only SeCO being produced but at 3-fold its intensity in nitrate-free media.[96] Based on the direct evidence
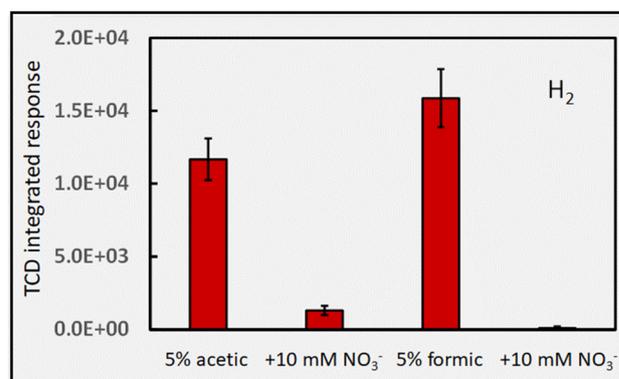
Fig. 8 Impact of the presence of 10 mM NO_3^- on HS H_2 response (generation) during photolysis of 5% (v/v) formic and acetic acids at 2 mL min^{-1} (IT = 22 s). Repeatability SD, $n = 3$. Ordinate displays integrated response characterizing chromatographic peaks.

This journal is © The Royal Society of Chemistry 2025

J. Anal. At. Spectrom., 2025, **40**, 70–97 | **83**

presented in Fig. 8 and the potential reactions (32)–(34), it is abundantly clear that efficient scavenging of H˙ radicals is responsible for this. Note also that the extent of H_2 generation from PVG media is typically insufficient to support atomization of hydrides in conventional heated quartz tube atomizers.[96,98]

Part 2: PVG in the presence of added TMs

Having gained fundamental insight into the influence of several experimental variables on the "baseline" photochemical production of stable small gas molecules from acetic and formic acid media, it is instructive to examine the impact of added transition metal ions (TMs). Their effects on precursor radical species that lead to H_2, CO, CO_2 and CH_4 may provide enhanced understanding of the mechanism(s) of action of these metal ion-assisted processes. As noted earlier, this study was not intended to be comprehensive, but rather limited to an examination of use of Cd(II), Co(II), Cu(II) and Ni(II) added to 5% (v/v) solutions of acetic and formic acids in an effort to minimize the complexity and number of experiments needed to be undertaken. For consistency, test solutions were irradiated at flow rates of 2 mL min^{-1}. An arbitrary but analytically efficacious concentration of each TM was identified from the more recent PVG literature related to use of flow-through photoreactors. Those perceived as having a significant influence on gas production were further examined by evaluation of their impact as a function of added concentration. It is acknowledged that further to their use with thin-film flow-through reactors, their beneficial influence has also recently been reported with use of standard (germicidal) low pressure mercury lamp sources limited to 254 nm output.[26,31,38,83,99]

Amongst the terminologies employed in the PVG literature, the use of TMs to enhance synthesis yields of targeted analytical species has variously been described as inducing a "photo-assisted" process due to the action of a "photocatalyst", a "photoredox catalyst" or a "photosensitizer". In view of the current paucity of mechanistic information, a more generalized description evoked by the phrase "TM-assisted" or "TM-mediated" is thus suggested for use herein, with a preference for the former terminology. By analogy, Kozlowski and Loon suggested that the most general term applicable to the entire field of TM-assisted reactions for organic synthesis be "photocatalysis", since the mechanism of energy transfer is typically unknown.[100]

TM-mediated gas production from formic acid

Generation of CO. Fig. 9 shows the change in CO production from 5% (v/v) formic acid induced by the presence of various concentrations of added Ni(II), Co(II), Cd(II) and Cu(II). During this experiment, unadulterated 5% formic acid generated a (uncorrected) concentration of 4290 ± 570 ppm (repeatability SD, $n = 3$), consistent with that reported earlier in Fig. 4, 7 and Table 1. Minor enhancements in CO are evident in the presence of added TMs, the largest effect accruing from added Cu(II) to produce a 50% increase in [CO] to 6550 ± 900 ppm (repeatability SD, $n = 3$). It is evident that each of the added TMs has an enhancement effect on CO production, although slightly different. More significantly, these generally small increases

appear insufficient to account for the typically order of magnitude increase in TM-mediated PVG analyte yields. A notable example is the 25% enhancement in [CO] in the presence of 20 µg mL^{-1} Cd(II). This minor increase in "reaction (reduction) partner" concentration is quite insufficient to account for an estimated 10 000-fold enhancement in PVG yield of $W(CO)_6$ elicited by its presence.[16] Such impact is more congruent with a catalytic than LMCT effect. Whereas Cd(II) is beneficial for PVG of W, Co(II) is completely ineffective and Cu(II) is reportedly 1000-fold less effective than that induced by the presence of Cd(II). As another typical example, the 4100-fold increase in yield of PVG generated Pb from formic acid following the addition of 6 µg mL^{-1} Ni(II)[13] can be realized despite the minor enhancement in [CO] produced with addition of 20 Ni(II) µg mL^{-1} to this medium, evident in Fig. 9. A further example is evident from the work of Hou et al., reporting that in the presence of 20 µg mL^{-1} of Co(II) or Cd(II), the PVG-ICP-MS response for Ru increased by 140- and 45-fold, respectively.[34] From the perspective of the small relative changes in the concentration of available CO as a reaction partner, it is not possible to readily account for these effects. Although TM reactions such as illustrated in eqn (26) may influence production of CO, the effects of such increases and their specificity are difficult to rationalize based on such simple scenarios. However, if the CO concentration in solution is sufficiently in excess of the target analyte during PVG in the
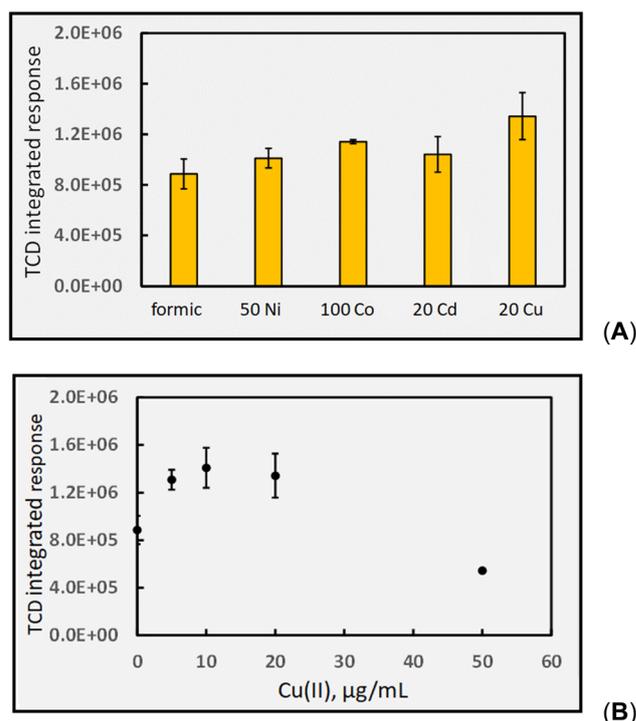

(A)

(B)

Fig. 9 Impact of added TMs (TM concentrations given as µg mL^{-1}) on HS CO response (generation). Photolysis of 5% (v/v) formic acid at a solution flow rate of 2 mL min^{-1} (IT = 22 s). Ordinate displays integrated response characterizing chromatographic peaks. (A) Uncorrected HS [CO] increases from 4290 ± 570 ppm to 6550 ± 900 ppm (repeatability SD, $n = 3$) in the presence of 20 µg mL^{-1} Cu(II). (B) Effect of increasing Cu(II) on HS CO response (generation).

84 | J. Anal. At. Spectrom., 2025, **40**, 70–97

This journal is © The Royal Society of Chemistry 2025

absence of added TM, then it will not be the rate limiting or critical reagent supporting synthesis. The impact of the presence of the TM on other gases, as proxies for radicals, must also be examined for a more holistic approach.

Selecting Cu(II) for further investigation, as it appears the most influential, Fig. 9B shows the effects of increasing concentrations of Cu(II) in the 5% formic acid medium on CO generation. In this example, the initial arbitrary selection of 20 $\mu g \ mL^{-1}$ shown in Fig. 9A was serendipitously close to that proving optimal in this system. Noteworthy is the overall shape of the function in that a maximum is present, reflecting the typical performance metric reported with all analytical PVG systems wherein the PVG yield of the targeted volatile metallic analyte species follows a similar profile noted here for the effects of added TMs.[13,16,20,24,27,32,34,35,82] The initial rate of increase with [Cu(II)] is short-ranged and one explanation frequently used to account for the decreasing efficiency at higher concentrations of added TMs is that their presence introduces an increasing shadowing effect whereby absorption of incident radiation due to TM d–d and charge transfer transitions of their carboxylate complex(es) inhibits primary photochemical reactions needed to generate the targeted analytical products. Unfortunately, it is rare that any additional absorption bands are identified in the UV spectra of TM adulterated PVG solutions and thus this argument is generally weak. Formation of Cu^0 NPs at high concentrations could lead to a scavenging of free CO and release of volatile Cu–CO species. In such situations, of course, the presence of Cu(II) in test samples at this concentration may likely be considered an interferant in the PVG process.

Further to this point, and in connection with the earlier introduced reaction 29 involving consumption of methyl radicals in the presence of NPs, it is instructive to consider the following general reaction which should be taken into consideration for synthesis of TM-carbonyls, as it often presents a practical limit to the issue of selecting the optimal concentration of added TM to effect the largest impact on the desired analyte PVG reaction while minimizing adverse effects:

$$TM^0 + nCO + (mH^\bullet \ or \ m/2H_2) \longrightarrow TM(CO)_nH_m \quad (36)$$
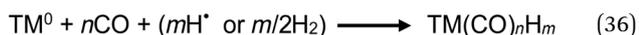
High concentrations of TM carbonyl compounds can result in significant contamination of mass spectrometer detection systems as they are employed at 10's of ppm or higher concentrations. An equally important consideration, however, is the impact of co-generation of such compounds on the consumption of available CO, H_2 or $H^\bullet$ species. A semiquantitative estimate of this effect may be undertaken using PVG generation of $Ni(CO)_4$ as an example. This is an analytically attractive process and occurs with high efficiency at trace concentrations. Assuming application of a 50 $\mu g \ mL^{-1}$ concentration of Ni(II) as a PVG mediator, as used in this study, significant amounts of $Ni(CO)_4$ would be generated. It is rather unlikely that this process continues with uniform high efficiency over such a broad concentration range, but if 50% is assumed, this would amount to a consumption of approximately 75 $\mu L \ min^{-1}$ CO during a typical photolysis

operation wherein only 320 $\mu L \ min^{-1}$ CO is photolytically generated in 5% (v/v) formic acid containing no added TMs (cf. earlier discussions of overall oxidation efficiency). This may represent a significant sink for available CO. Similar calculations come into play considering hydrogen and methane. Very likely, PVG of TM carbonylated species occurs with significantly lower efficiencies at concentrations orders of magnitude higher than heretofore examined under analytical PVG concentrations. However, it is possible that actual generation of CO and H_2 via photolysis may be significantly higher (by up to 50%) in the Ni(II) and Co(II) systems studied here than is represented in Fig. 9 and 10 (below) due to its competitive uptake (apparent loss) as a TM carbonyl compound. In this connection, it would be of interest to determine residual TM content in the waste solutions of photolysed media.

Generation of H_2. Examination of this same suite of TMs added to 5% formic results in a significantly different pattern of results for the production of H_2, ranging from insignificant changes with added Cd(II) and Ni(II) to an 8-fold enhancement in the presence of Cu(II), as shown in Fig. 10A.

The issue arises as to what means, in an otherwise identical system, can the products of photolysis be so significantly altered with regard to CO or H_2 for a given added TM ion; again, LMCT reactions are completely inconsistent in this regard.

Fig. 10B shows the impact of [Cu(II)] on H_2 generation. As with CO generation, an optimum concentration is evident, suggesting a possible common origin. The relatively rapid drop in enhanced production of CO and H_2 with a further increase in added Cu(II) cannot be accounted for by either spectral shadowing or invoking a LMCT model of enhanced radical production, despite interpretation of ESR evidence, which unfortunately has never been quantitatively investigated.

A further observation that is not possible to rationalize is the synergistic effect of co-addition of two TMs to the sample solution, a frequent observation in the more recent analytical PVG literature wherein combination of individual TMs provides for an enhanced synthesis of targeted analytes beyond the summed impact of either.[6,33–36] Fig. 11 illustrates the synergistic impact of the simultaneous presence of both Co(II) and Cd(II) in a 5% solution of formic acid wherein the yield of H_2 is clearly greater than the sum of the impact of either TM alone. Obviously, if each TM-formate complex contributes to an enhanced production of radicals through their associated LMCT processes, it is difficult to account for a synergistic effect when both are present; the mechanism itself must be altered.

Generation of CO_2. The presence of added TMs appears to have no remarkable effect on the yield of CO_2 from 5% formic acid, as shown in Fig. 12, again pointing to the possible specificity of the impact of added TMs on production of the various stable gas species. Selecting Cu(II) for study of its concentration dependence also reveals no significant trend, generating only a further 20% increase at higher (50 $\mu g \ mL^{-1}$) concentrations.

TM-mediated gas production from acetic acid

Generation of CH_4. All added TMs influence generation of CH_4 and, with the exception of a 40% suppression caused by 20

This journal is © The Royal Society of Chemistry 2025
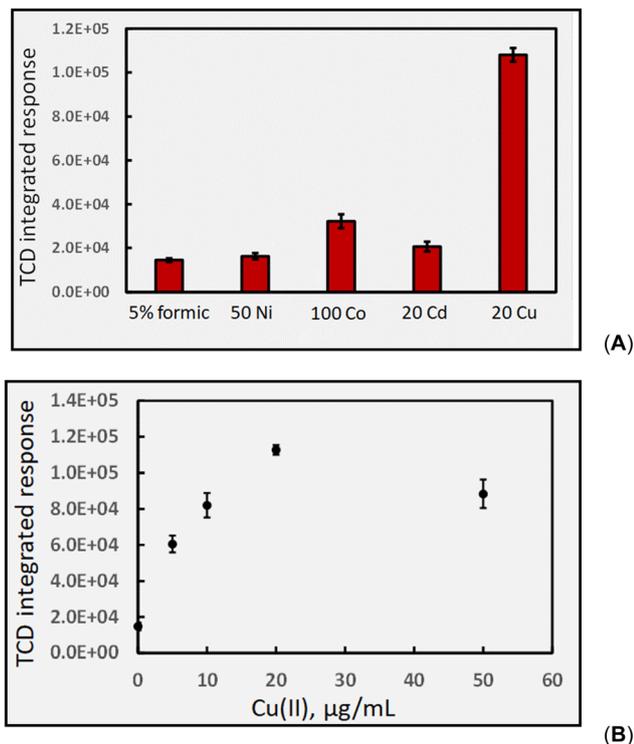
J. Anal. At. Spectrom., 2025, 40, 70–97 | 85

Fig. 10 Impact of added TMs (TM concentrations given as µg mL^{-1}) on HS H$_2$ response (generation). Photolysis of 5% (v/v) formic acid at a solution flow rate of 2 mL min^{-1} (IT = 22 s). Ordinate displays integrated response characterizing chromatographic peaks. (A) Uncorrected HS [H$_2$] increases from 370 ± 20 ppm to 2880 ± 80 ppm (repeatability SD, $n = 3$) in the presence of 20 µg mL^{-1} Cu(II). (B) Effect of increasing Cu(II) on HS H$_2$ response.

µg mL^{-1} Cu(II), give rise to increased yields (up to 75% with added Co), as illustrated in Fig. 13. This observation is both surprising and unique, considering the effectiveness of Cu(II) in enhancing the generation of all gases of interest in the formic acid system (cf. Fig. 9, 10 and 12). This further highlights the severe limitations of invoking generalized beneficial LMCT
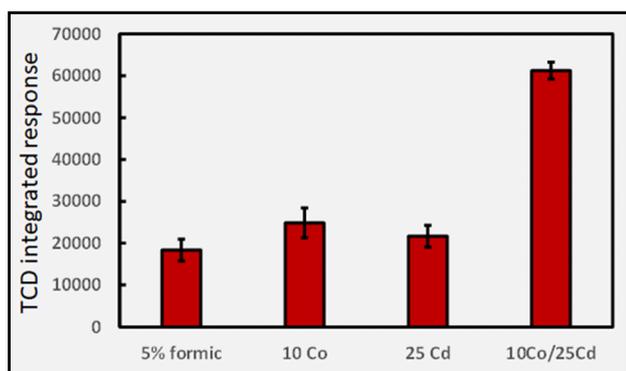

Fig. 11 Synergistic effect of the simultaneous presence of two TMs (concentrations given as µg mL^{-1}) on HS H$_2$ response (generation) during photolysis of 5% (v/v) formic acid at a solution flow rate of 2 mL min^{-1} (IT = 22 s; repeatability SD, $n = 3$). Ordinate displays integrated response characterizing chromatographic peaks.
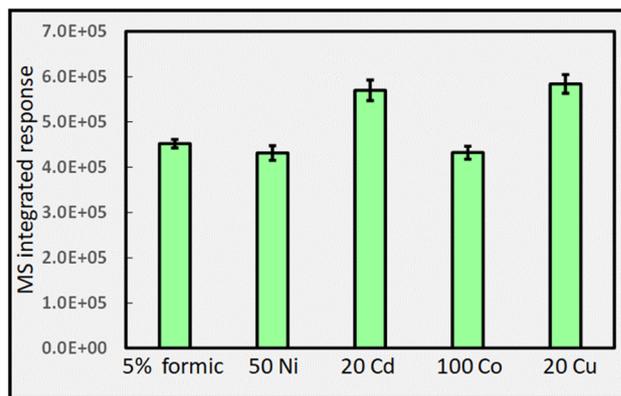

Fig. 12 Impact of added TMs (concentrations given in µg mL^{-1}) on HS CO$_2$ response (generation) during photolysis of 5% (v/v) formic acid at a solution flow rate of 2 mL min^{-1} (IT = 22 s; repeatability SD, $n = 3$). Ordinate units are integrated response over chromatographic peak.

reactions to account for TM-mediated enhanced yields of targeted analytical PVG species; it is evident that TM specific interactions with the carboxylate medium, its radical products of photolysis, as well as possibly the precursor analyte species, may all be at play.

As Co(II) appears most beneficial for CH$_4$ generation, the impact of varying its concentration was examined in the range 0–200 µg mL^{-1}. An optimum was evident near 75 µg mL^{-1}, beyond which response decreased, reaching 70% of maximum at 200 µg mL^{-1}. This pattern produced by increasing TM concentrations remains consistent with all other gases generated in the formic acid system as well as being reflected by their impact on analyte targeted analytical PVG systems.

The use of a mixture of added Cd(II) and Co(II) (25 and 10 µg mL^{-1}, respectively) on CH$_4$ production did not lead to a synergistic effect, providing the same response as that from 25 µg mL^{-1} Cd(II) alone. In accordance with the possible existence of an ionic bimetallic-coupled photoredox catalytic cycle,[44] such a TM mixture, demonstrated to occur for one analytical PVG system, should be viable in all, irrespective of the intended analyte target.
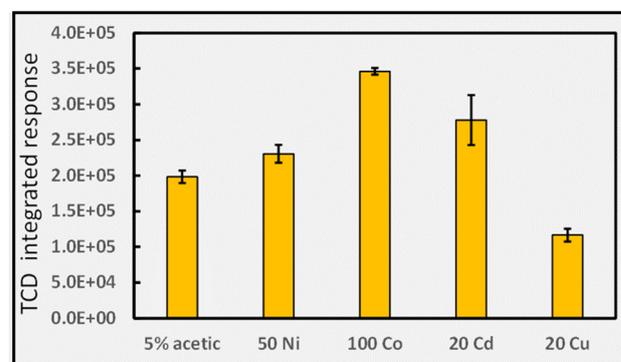

Fig. 13 Impact of added TMs (concentrations given as µg mL^{-1}) on HS CH$_4$ response (generation) from photolysis of 5% (v/v) acetic acid at 2 mL min^{-1} (IT = 32 s; repeatability SD, $n = 3$). Ordinate displays integrated response characterizing chromatographic peaks.

86 | *J. Anal. At. Spectrom.*, 2025, **40**, 70–97

This journal is © The Royal Society of Chemistry 2025

As earlier discussed in relation to Fig. 6B, photolysis of acetic acid generates C_2H_6 as a consequence of reaction 19. The impact of added Co(II) in the range 0–200 μg mL^{-1} on C_2H_6 generation was remarkable in that it provided a rather monotonic decrease in C_2H_6 response from 1080 ± 160 (repeatability SD: $n = 4$) to 690 ± 50 ($n = 4$). Clearly, the reaction is influenced by the presence of Co(II) but the mechanism of action is unclear since, as shown in Fig. 13, Co(II) enhances CH_4 production (implying enhancements in precursor $^•CH_3$ production) but its presence apparently inhibits reaction (19).
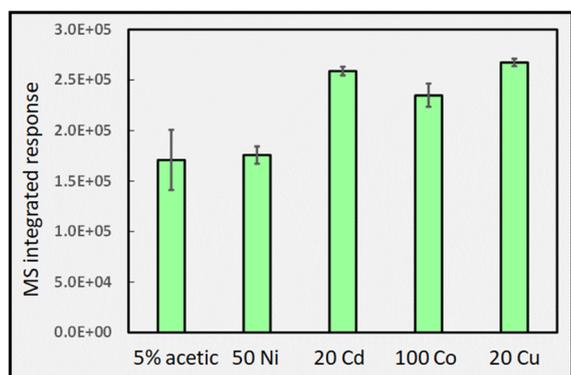
Generation of CO_2. With the exception of Ni(II), small enhancements (<30%) in CO_2 generation arise in the presence of each of the other TMs under study. Although Cu(II) suppressed production of CH_4, it was one of the more efficacious TMs contributing to CO_2 production, as shown in Fig. 14A.

Fig. 14B shows the typical impact of increasing Co(II) concentration on CO_2 generation, once again illustrating the presence of a generic optimum that is also reflected in the analytical PVG literature for generation of volatile species of all targeted analytes, as discussed earlier.
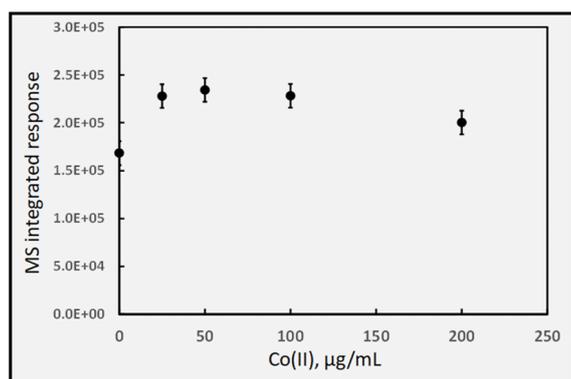
Generation of CO. As noted earlier, the source of CO during the photolysis of acetic acid remains unclear as there is no evident photolysis route to directly generate this gas (neither photolytic nor thermal). A low formic acid impurity could readily account for the detected 14 ± 4 ppm HS (uncorrected) concentration produced in 5% acetic acid solutions, as discussed in relation to Fig. 5B. The impact of added TMs mirrors that observed for the production of CO in formic acid (Fig. 9) in that enhancements of <50% occur in the presence of each added metal; the (uncorrected) HS concentration remains in the range <30 ppm. As noted in Fig. 9B, higher concentrations of added TMs [in this case Cu(II)] suppressed CO production and in the 5% acetic acid medium an increase in added Co(II) from 100 to 200 μg mL^{-1} reduced the HS CO concentration to its value in the absence of added TMs.

Generation of H_2. In stark contrast to the formic acid system (Fig. 10), H_2 production in 5% acetic acid is suppressed by all added TMs, most notably by the presence of Cu(II), as shown in Fig. 15. As methylated metal (and halogen) species are the typical products of analytical PVG in acetic acid, any changes in H_2 production should not have apparent impacts on targeted element analytical response. In any event, this observation is contrary to all expectations based on a LMCT model which suggest increased radical precursors to H_2 generation (*cf.* reaction (24)).
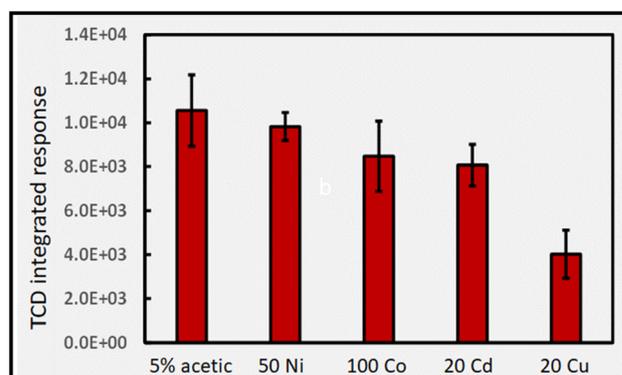

Fig. 15 Impact of added TMs (concentrations given as μg mL^{-1}) on response (generation) of H_2 from photolysis of 5% (v/v) acetic acid at 2 mL min^{-1} (IT = 32 s; repeatability SD: $n = 3$). Uncorrected HS [H_2] in 5% acetic acid is 270 ± 40 ppm. Ordinate displays integrated response characterizing chromatographic peaks.

Although a synergistic effect on H_2 production was very pronounced when a combination of Co(II) and Cd(II) was present in 5% formic acid (*cf.* Fig. 11) no such trend arises when the experiment is replicated using 5% acetic acid, highlighting the uniqueness of catalyst substrate/reactant interactions in changing from formic to acetic acid.

Part 3. Possible mechanisms of action of added TMs

A general model based on enhanced radical production in formic and acetic acids in the presence of added TMs is supported by direct ESR evidence (mostly limited to $^•CH_3$ and $CO_2^{•-}$ with a single report for H$^•$[62]). LMCT reactions involving TM-carboxylate complexes efficiently harvest longer wavelength photons from the photoreactors, potentially leading to more

Fig. 14 (A) impact of added TMs (concentrations given as μg mL^{-1}) on response (generation) of HS CO_2 during photolysis of 5% (v/v) acetic acid at 2 mL min^{-1} (IT = 32 s). Ordinate displays integrated response characterizing chromatographic peaks; (B) effect of added Co(II) on HS CO_2 response (generation). Uncorrected HS [CO_2] increases from 1670 ± 100 ppm to 2160 ± 40 ppm (repeatability SD, $n = 4$) in the presence of 100 μg mL^{-1} Co(II).

This journal is © The Royal Society of Chemistry 2025

J. Anal. At. Spectrom., 2025, **40**, 70–97 | **87**

favorable PVG reaction kinetics. However, this study exposes several shortcomings with use of this model:

(i) A limitation or saturation in the magnitude of the analytical effect as the concentration of TMs is increased as generally exhibited by an asymptotic impact profile that is not likely due to spectral shadowing (minimal effect in the UV-B region supporting LMCT processes) and generally fails to reveal evidence of any significant or distinctive TM-carboxylate LMCT bands in examined UV-Vis spectra of TM-spiked PVG solution media which could account for their action; note that PVG halide systems display broad concentration ranges over which added TMs do not result in decreased synthesis efficiencies, highlighting a distinctly different mechanism of action.

(ii) A specificity of effects unique to particular TM-analyte combinations is evident in the PVG literature; in accordance with a generalized LMCT model, a positive impact should be expected which transcends specific TM-analyte combinations as no perturbation to the photochemical system is made apart from the addition of a TM; such specificity cannot be accounted for by LMCT processes and appears equally evident in the impact of specific TMs affecting yields of stable gases which arise from radical precursors.

(iii) Synergistic interactions amongst added TMs cannot be accounted for based on LMCT reactions proportionally contributing to the population of "radical reagents"; a simple sum of the effects of each is expected due to their independence; as noted earlier, possible ionic bimetallic-coupled photoredox catalytic cycles[44] may occur, but should remain effective irrespective of the coupled analyte target.

(iv) Inconsistent effects amongst the generation patterns of gases in the presence of the various TMs occur, a most dramatic example being a decrease in methane and hydrogen production in the presence of Cu, which cannot be accounted for by LMCT events.

(v) Catalytic redox cycle reactions, such as those proposed by Adams and Hart[60] involving the presence of variable valence TMs (*i.e.*, reactions (26)–(28)), may occur with photolytically generated radicals such as $^{\bullet}COOH$ and $HCOO^{\bullet}$ enhancing rates of generation of CO and CO_2, but this effect (at least for Ni, Co, Cd and Cu) is quantitatively small (<30% change) for both CO (Fig. 9) and CO_2 (Fig. 12) and any such increases in intermediate reducing radicals would not be expected to yield major enhancements in PVG analyte efficiencies.

An alternative model that may more comprehensively and consistently account for all of the above suggests intervention by homogeneous generation of (photo)catalytic nanoparticles (NPs) from the added TMs. Their formation during the PVG process cannot be disputed; they have been visually evident, as reported by the formation of pink-colored Se^0 deposits when formic acid solutions containing mg L^{-1} concentrations of Se(IV) are subjected to PVG[96] and, more recently, identified as being present in several PVG systems by TEM imaging techniques.[24,33,37,101,102] A most recent example, presented in Fig. 16, shows islands or clusters comprising bimetallic Cd and Co NPs isolated from a mixture of 50 μg mL^{-1} Cu(II)/100 μg mL^{-1} Co(II) in 0.045% (v/v) formic acid following PVG. Individual NPs

typically appear to be <5 nm in diameter within their 50 nm clusters.

Although single particle ICP-MS (SP-ICP-MS) would seem to be a convenient technique for detection of such NPs, no such reports have appeared, possibly because of insufficient detection power due to their small size (<10 nm) coupled with the elevated background arising from the high dissolved ionic fraction of 10's of mg L^{-1} added TMs.[103,104] It would appear that, for the selected TMs used in this study (Ni, Co, Cd and Cu), current SP-ICP-MS detection approaches are not tenable (note that the 50 nm islands shown in Fig. 16A would be disaggregated prior to applying SP-ICP-MS due to commonly used sample preparation techniques).

Catalytic (thermal) processes can broadly be characterized as either associative or redox. With the former, one or more reactant molecules are adsorbed onto active surface sites in such an energetically favorable environment that intermediates form and products desorb. The latter redox mechanism engages changes in oxidation state of the catalytic material innate to their variable valence states, such as involvement of surface oxygen vacancies. In both cases, initial adsorption or surface interaction is inherent to the catalytic process and efficiencies
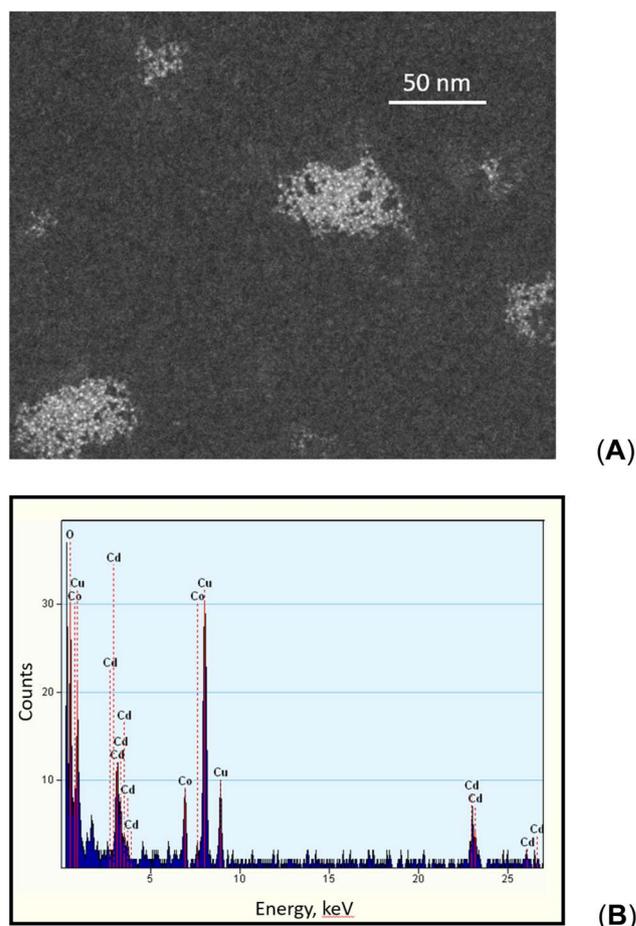

(A)

(B)

Fig. 16 (A) TEM image of clusters of mixed Cd/Co comprising NPs of diameter < 5 nm synthesized during PVG of 0.045% (v/v) formic acid containing 50 μg mL^{-1} Cd(II)/100 μg mL^{-1} Co(II); (B) EDX profile of a cluster (images courtesy of M. Couillard, EME/NRC).

88 | *J. Anal. At. Spectrom.*, 2025, **40**, 70–97

This journal is © The Royal Society of Chemistry 2025

are influenced by the Sabatier principle. In the context of PVG, which is driven by UV-C irradiation, it is evident that excited states of reactant molecules are already engaged to homogeneously produce the needed radicals that lead to analytical products in the absence of added TMs. Addition of TMs to this system may, in successful cases, result in production of TM NPs and photocatalytic effects associated with excitation of electron–hole pairs either within their conduction band (intraband excitation) or between the d-band and the conduction band (interband excitation) where they can reduce surface-adsorbed species or serve as oxidizing agents, allowing redox processes to occur at lower UV energies and with higher efficiency by utilizing longer wavelength source radiation.[105] Most recent evidence favors the role of interband transitions.[106] In this vein, it may be possible to imagine a scenario akin to electro-photocatalysis[75] wherein the SC properties of the TM and/or transition metal oxide (TMO) NPs serve to establish the electrochemical potentials helping to drive reactions of surface adsorbed species.[107]

Such significant impacts of heterogeneous SC and MOF additives are already well-appreciated and utilized across many fields of photochemical research and application. Specifically, early PVG studies reported extensive use and performance enhancements arising from the presence of nano-TiO_2 and noble metal decorated TiO_2 systems.[7,8,10,29,108] These structures facilitate rapid reactions on their surfaces to which the reaction partners have adsorbed, and make more efficient use of photogenerated electrons as a consequence of their electronic bandgaps, as detailed by Amal and colleagues in the case of Se(VI),[109] to provide more energetically favorable routes for radical generation. ESR studies have corroborated enhanced photochemical yields of $CO_2^{\bullet-}$ in formic acid[47] and $^{\bullet}CH_3$ in acetic acid[48] in the presence of added SCs.

Zou et al.[12,110] have summarized uses of not only conventional heterogeneous catalysts such as MOFs and TiO_2, but also homogeneous "catalysts" based on TMs added to PVG systems. However, no mechanistic pathways were proffered by which the latter actually functioned or could be justified to be addressed as "catalysts".

In contrast to their heterogeneous counterparts (primarily TiO_2 to date), the size, shape and composition of metallic NPs significantly affects their catalytic performance; as they become smaller, new chemical and physical properties emerge as specific surface areas increase along with increases in reactive edge, step and corner sites. Below some critical particle size, changes also occur in their electronic structures which become more quantized, leading to discrete electronic states rather than those of a continuous spectrum in a macroscopic bulk metal.[111–113] Correspondingly, their size influences not only their impact on reaction rates, but also product selectivity as they possess varying crystallographic structures which have implications for chemical reactivity. Exchange interactions of adsorbate electrons with conduction band electrons alter the NP surface electron density, affecting the adsorption of the surface-bound species as well as the wavelength of the localized absorption band (Localized Surface Plasmon Resonance, LSPR), potentially controlling synthesis products as well as selectivity

of the adsorber.[114] Decay of resonant surface plasmons may result in direct excitation of an electron to an unoccupied adsorbate acceptor state, weakening the chemical bonds within the adsorbate to induce dissociation of the adsorbed species. Even in TM NPs lacking strong plasmonic resonance due to their unfilled d-orbitals, interband excited electrons in these metal NPs can facilitate reactions at the NPs' surface via visible light excitation.[106]

The ubiquitous presence of dissolved oxygen ($\sim$8 mg L^{-1}) and its consequent photolysis by-products (e.g., $O_2^{\bullet-}$ or $HO_2^{\bullet}$) in PVG media suggests two potential roles. Firstly, the nascent TM atoms or their clusters may readily form TMO species (and binary TMOs with mixed TMs) with SC properties analogous to the well-known TiO_2 discussed above.[115] Such TMOs have also been actively utilized to promote catalytically enhanced redox reactions by nature of the variable valence properties of elements such as Cu, Ni, Co and Fe and numerous vacancy sites on their surfaces.[116,117] Possible redox (electrochemical) reactions needed to reduce targeted analytical species during PVG could be catalytically enhanced in the presence of TMOs, aiding the homogeneous photoreduction reactions ascribed to $H^{\bullet}$, $R^{\bullet}$, and $CO_2^{\bullet-}$. Second, dissolved oxygen may play a direct role in a catalytic cycle wherein excited photogenerated surface electrons may react with O_2 to create positively biased NP surface sites that foster adsorption of anionic partners (i.e., ionized carboxylate species) to further promote overall reactions.[118]

Over the past few decades, numerous organic and inorganic reactions have been catalyzed using both colloidal (free) and supported TM and TMO nanocatalysts[105,119–122] with a maximum in utilization and selectivity culminating in the extreme of (host matrix supported) single atom catalysts.[123–125] Synthetic organic chemists are currently making significant use of the photochemistry of formate salts to perform the roles of reductant, carbonyl source and hydrogen atom transfer reagent in a variety of reactions.[126] Correspondingly, it is not surprising that interest in their application to inorganic PVG systems has surfaced. With the above properties in mind, a model based on the impact of in situ photoreductive synthesis of TM NPs in PVG systems should be explored to more comprehensively rationalize observations reported in this study, as well as account for those in the recent PVG literature to a better degree than can be achieved using the current LMCT model.

It is clear that as NP catalysts exhibit significant size-dependent photoactivities,[105] this property naturally gives rise to an optimum particle size distribution whose effects may vary, depending on the PVG analytical target, due to the need for simultaneously compatible surface interactions. Additionally, the spectral output of the photoreactor likely plays a role in determining the optimal NP size as there will be a trade-off between the impact of available photon intensity and the efficiency of its LSPR effect. In the flow-through photoreactor, time-dependent development of an optimal NP size distribution will be directly influenced by the initial concentration of the added TM. Whereas the precise mechanism and kinetics of formation of reduced atoms in solution and their agglomeration remains largely unknown for most systems, recent studies suggest that following initial reduction to atoms, small semiconducting clusters form

This journal is © The Royal Society of Chemistry 2025

J. Anal. At. Spectrom., 2025, **40**, 70–97 | **89**

which rapidly transition to plasmonic nanoparticles *via* agglomeration.[127,128] An optimal TM solution concentration is thus to be expected and has been reported in every successful application of a TM-mediated PVG system. Decreasing performance characteristics at higher concentrations, often attributed to spectral shadowing effects, more likely manifests due to time dependent changes in NP size which alter the selective adsorption interactions of reactants onto the NPs. This is also mirrored in their influence on the relative yields of the photolysis gas products, as investigated in this study. It is expected that such TM concentration dependencies are unique and differ in range with different TMs and, by consequence because of their specificity of developed surface properties, also vary with the PVG analyte target; a TM most suitable for one PVG analyte may exhibit completely different performance characteristics with a different analyte, as attested to in the PVG literature.

Use of specific combinations of added TMs leading to unique synergistic impacts on PVG efficiencies is also readily rationalized by recognizing that bimetallic NPs can distinctively enhance catalytic properties for radical production as compared to those of their monometallic constituents.[111,114,116] They would also be expected to exhibit diverse catalytic effects on different PVG analyte systems due to specific surface adsorption phenomena, consistent with observations in the PVG literature[6,33–36,45] and in the general field of catalysis wherein small alterations to bi- or multi-metallic catalyst composition may significantly change desired performance.[129,130]

The addition of Cu(II) to formic acid significantly increases the yield of H_2 (*cf.* Fig. 10) whereas the opposite occurs in the acetic acid system [decreasing both CH_4 (Fig. 13) and H_2 (Fig. 15)]. It has been reported that (photolytically generated) precursor radicals can be captured by suspensions of TM NPs in aqueous media, leading to their reduction and formation of long-lived NP-$(CH_3)_x$ and NP-H_x surface species.[73,74,131] Adsorption of H$\cdot$ onto the Cu^0 NP surface fosters their desorption as H_2 in a classical heterogeneous catalytic mechanism, thereby accounting for the enhanced H_2 production. In acetic acid, additional reactions may occur due to the presence of $\cdot CH_3$ and a much smaller population of H$\cdot$ (possibly arising from photolysis of HCOOH impurity) to make this matter more complicated. Co-adsorption of $\cdot CH_3$ and H$\cdot$ would lead to

production of a small increase in CH_4 and a substantial decrease in H_2 production due to the excess $\cdot CH_3$ in this system. Despite this, an overall decrease in CH_4 generation may be arise due to reaction of adsorbed $\cdot CH_3$ with adjacent water molecules to produce CH_3OH. Post photolysis thermal reactions of generated radicals in the acetic acid system are more varied than in formic acid.

In this adsorbed state, a variety of reactions, including those with adsorbed CO_2, may proceed to yield acetic acid with a concurrent reduction in generation of CH_4, H_2 and C_2H_6.[132] It is acknowledged that the cited publication (ref. 132) refers to a nonaqueous thermal reaction, but the principle reactions may still occur in the PVG system and would, moreover, be dependent on the TM NP composition and hence reflect the variable impact of the different TMs (and their combinations) examined in this study. Clearly, interpreting the impact of TMs *via* the LMCT model cannot account for any of the above observations.

In an effort to present a visual summary of the results, a chemometric analysis of the relative impact of the addition of each TM mediator on each measured gas in both acid media was attempted. Hierarchical Cluster Analysis (HCA), an unsupervised pattern recognition chemometric tool, was performed using MetaboAnalyst 6.0 software (freely available at **https://www.metaboanalyst.ca**) to highlight any patterns that may be present. Uncorrected HS concentrations generated for each gas in the presence and absence of added TMs represented the sample input data. The gas concentrations were normalized, using auto-scaling, by which the data were centered on their mean divided by its standard deviation in each carboxylic acid. Such data pre-processing was necessary to ensure that all samples were accorded the same weight in subsequent treatment. After pre-processing, the (Euclidean) distances amongst the samples (original single point "clusters") were calculated and interconnected using a Ward D linkage algorithm based on minimum variance when merging clusters. Fig. 17 summarizes the results wherein concentrations are reflected as colors (the deepest red representing highest while deepest blue reflects the lowest) and the horizontal and vertical lines comprise the dendrograms, *i.e.*, summaries of the distance matrix. It is evident that the HCA treatment readily identifies which added TM has had the greatest impact on
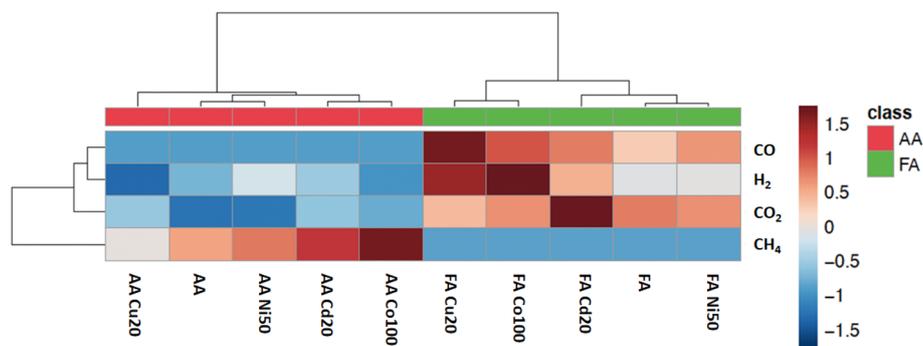

Fig. 17 HCA results depicted as a "heatmap" (Euclidean distances for clustering algorithm using Ward D methodology). AA: 5% (v/v) acetic acid; FA: 5% (v/v) formic acid; element and number designations represent added transition metal mediator to the PVG medium at the indicated concentration in μg mL^{-1}.

relative generation of a given gas compared to photolysis of the "unspiked" 5% (v/v) acid system. As examples, in a 5% (v/v) formic acid medium, FA Cu20 (*i.e.*, 20 μg mL^{-1} Cu^{2+} added) revealed greatest impact on the generation of elevated concentrations of CO compared to its effect on the other gases; however, the highest concentration of H$_2$ was obtained using FA Co100, and for CO$_2$, FA Cd20 is unique. Turning to the 5% (v/v) acetic acid system, it is clear that greatest increase in concentration of CH$_4$ occurs in the presence of 100 μg mL^{-1} added Co, *i.e.*, AA Co100. Most significant is that overall, the impact of each added TM is unique for each gas in each acid and no clusters can be identified.

Conclusions and future studies

A complementary and novel approach to the usual direct observation of the impact of added TMs on the synthesis yields of PVG target analytes is presented here based on their effects on changes in the relative concentrations of generated H$_2$, CO, CH$_4$ and CO$_2$ as stable end products of photolysis. Reducing radicals currently envisioned as responsible for analytical PVG processes (•H, e$_{(aq)}^-$, •CH$_3$, CO$_2$•$^-$) are also precursors to these gases along with CO, permitting use of this new tool for such investigations. A photocatalytic mechanism mediated by homogeneous co-generation of TM/TMO nanostructures has been proposed which may more comprehensively account for their reported analytical effects than is possible *via* LMCT processes, particularly the notable selectivity accompanying improved PVG efficiencies of specific analytes.

In contrast to frequent high and robust vapor generation efficiencies for numerous analytes, oxidation of formic and acetic acids (and corresponding radical production) appears to be very inefficient. Despite use of state-of-the-art flow-through photoreactors, overall oxidation does not exceed 1% under typical operating conditions. However, with the low concentrations of analytical targets (~100 ng mL^{-1}), generation of a 10^4-fold excess molar ratios of active radicals can readily account for high synthesis efficiencies of targeted metals and halogens.

The overall impact of added TMs likely derives from a combination of enhanced reaction rates arising from the *in situ* formation of (photo)catalytic TM/TMO structures coupled with an acknowledged background of LMCT reactions, both contributing to increased production of reducing radicals. However, very substantially increased synthesis yields of analytical targets amounting to more than an order of magnitude, and those exhibiting a synergistic response to specific combinations of added TMs, can more likely be attributed to the intervention of *in situ* generated catalytic surfaces.

Hou and colleagues[37] noted that whereas CdSe, CdTe and CdS nanocatalysts were each able to catalyse the PVG generation of Se(CH$_3$)$_2$ from Se(VI), ZnS was distinctly inactive. This led to the conclusion that the metal centre of the SC catalyst (*i.e.*, Cd) is key to successful use. This supports the high specificity of TM-NP-target analyte interactions. Clearly, significantly more work is required to investigate the impacts and actual mechanisms arising from addition of TMs to PVG systems. For comparison, the most common SC TMO in use, TiO$_2$, should be examined for

its influence on the profiles of generated stable gases. Building on the work of Amal *et al.*,[109] and the purported mechanisms of action revealed for reduction of Se(VI), it would be of interest to determine in what manner this catalyst and its metal decorated forms perturb the stable gas profiles. Interestingly, these may be significantly altered in the presence of TiO$_2$.[71,133] Dey *et al.*[133] reported that, in addition to the usual H$_2$, CO and CO$_2$ arising from photolysis of formic acid, a small yield of CH$_4$ was also detected and putatively accounted for by chemical reduction of CO$_2$. Although Gao and colleagues[29] suggested that a synergistic interaction was evident for PVG of Te when iron was added to a mixture of acetic and formic acids containing TiO$_2$, more likely TM NPs of reduced Fe were sequestered onto the existing catalyst surface to alter its Fermi level and provide for a more efficient reducing environment consistent with the characteristics of such a "decorated" catalyst.

The influence of solution pH was not examined in this study. Considering that pH is one of the most effective variables influencing not only the degree of ionization of the carboxylic acids, but the electrical charge characteristics of possible catalytic surfaces and thereby their affinity for adsorption of species, it may play a critical role governing the action of resultant TM-NPs and should be examined in detail as it may also influence the growth and lifetime of the NPs.

Potential losses of detected gaseous products of PVG may arise as a result of their precursor radical constituents participating in various competitive parallel thermal reactions. This was shown to be the case for methanol, which induced a small negative bias in detected CH$_4$ concentrations in photolysed acetic acid and was implicated in potential loss of CO by formation of acetaldehyde during photolysis of formic acid. The concentration profiles of such water miscible products under various experimental conditions, notably in the presence of added TMs, need to be examined to more comprehensively expand the scope of this study to more rigorously account for any additional loss mechanisms for CO as well as CH$_4$ and H$_2$ proposed earlier in the presence of Cu^0.

It would be of interest to contrast the results of this study with those obtained using a non-ozone generating low pressure photoreactor, precluding vacuum UV output and limited to wavelengths >254 nm, to ascertain whether the same trends are evident. Such a study is also interconnected with an evaluation of interference effects arising from TMs and whether any resulting NPs formed serve to enhance or mitigate interferences such as those due to nitrate/nitrite.

In this connection, these gas studies should be augmented with results generated from aerated and deoxygenated systems. This aspect is not currently controlled during PVG, despite being a potentially significant variable that may contribute to analytical PVG interference alleviation as well as alteration of the profile of gas production due to changes in the mechanisms of photolysis itself, as reported by Dey *et al.* during a study of TiO$_2$ mediated photolysis of formic acid.[133]

Lastly, and likely of most immediate importance to the present discussion, more effort directed to detection and characterization of proposed TM/TMO species utilizing microscopic and optical techniques such as TEM, dynamic light scattering

This journal is © The Royal Society of Chemistry 2025

J. Anal. At. Spectrom., 2025, **40**, 70–97 | 91

(DLS),[134] asymmetric flow field-flow fractionation with multi-angle light scattering (AF4-MALS)[135] and (nano)particle tracking analysis (NTA)[136] are needed in order to more convincingly underpin the foundations of this model. TEM imaging is potentially influenced by sample preparation techniques and is done off-line, typically *via* evaporation of a small volume of the photolysed sample onto a supporting grid, inviting the possibility of post-photolysis NP growth and nucleation (or even their dissolution) or interference from simple crystallization of the concomitant excess TM salt. DLS, on the other hand, can be readily configured for continuous on-line examination of the effluent from the GLS in real time, without operator intervention, providing particle size and distribution data in the range 1–1000 nm. NTA further provides information on particle size distribution in the range 10–1000 nm and number density of typically 10^6–10^9 cm^{-3}. To place this latter metric into perspective, if an added 50 μg mL^{-1} Co(II) concentration is under investigation and assumed to be quantitatively transformed into 10 nm particles during photolysis, the resultant number density would be 1×10^{13} cm^{-3}. Provided only 10^{-5}% fraction was so formed, this would still be within the particle density range for NTA detection. As discussed earlier, although SP-ICP-MS may appear to be an ideal tool for such investigations, the current lack of any results supported by this technique may simply point to insufficient detection power if the responsible nanoparticles prove to typically be <10 nm in diameter.

Apart from the proposal that TM NPs are strongly implicated in the action of TM-mediated PVG, no description of an explicit mechanism by which this occurs has been advanced herein, aside from arguments suggesting that the analytical target ion or carboxylate complex is likely involved in order to account for the high specificity of effect with different TMs. Such mechanisms are beyond the scope of this work and need to be elucidated, but guidance may be drawn from the increasing literature devoted to metallaphotocatalysis of TMs under visible light to foster numerous organic reactions[137,138] as well as a better understanding of the influence of metals used for catalyst decoration on available reactive electron species.[139] In this connection, the influence of reaction wavelength requires attention, as initially investigated by Hou and colleagues for the limited case of PVG of Se wherein the attributes of a laser driven light source were highlighted as an ideal tool for this purpose.[140]

As with earlier complementary tutorials on PVG,[3,4] this contribution bears a significant shortcoming in that it has neither proved nor disproved any proposed fundamental mechanisms. However, it aspires to provide a potentially more coherent framework with which to rationally approach the subject of TM-mediated PVG while hopefully enticing interested researchers and experts from complementary disciplines to conduct further investigations of many of the intriguing facets presented herein which will contribute to the continuing advancement of this field.

Data availability

Data supporting the experimental findings of this study are presented within the article; those mentioned by way of a simple summary statement are available from the corresponding author upon reasonable request.

Author contributions

Conflicts of interest

The authors declare that there are no conflicts of interest associated with this manuscript.

Acknowledgements

References

1 *Vapor Generation Techniques for Trace Element Analysis: Fundamental Aspects*, ed A. D'Ulivo and R. E. Sturgeon, Elsevier, 2022 ISBN: 9780323858342.

2 R. E. Sturgeon and P. Grinberg, Some speculations on the mechanisms of photochemical vapor generation, *J. Anal. At. Spectrom.*, 2012, **27**, 222–231.

3 R. E. Sturgeon, Photochemical vapor generation: a radical approach to analyte introduction for atomic spectrometry, *J. Anal. At. Spectrom.*, 2017, **32**, 2319–2340.

4 D. Leonori and R. E. Sturgeon, A unified approach to mechanistic aspects of photochemical vapor generation, *J. Anal. At. Spectrom.*, 2019, **34**, 636–654.

5 R. E. Sturgeon, Photo-sono-thermo-chemical vapor generation techniques, in *Vapor Generation Techniques for Trace Element Analysis: Fundamental Aspects*, ed A. D'Ulivo and R. E. Sturgeon, Elsevier, 2022 chapter 7.

6 Y. Zhen, H. Chen, M. Zhang, J. Hu and X. Hou, Cadmium and cobalt ions enhanced-photochemical vapor generation for determination of trace rhenium by ICP-MS, *Appl. Spectrosc. Rev.*, 2022, **57**, 318–337.

7 E. Kikuchi and H. Sakamoto, Kinetics of the reduction reaction of selenate ions by TiO$_2$ photocatalyst, *J. Electrochem. Soc.*, 2000, **147**, 4589–4593.

8 Q. Wang, J. Liang, J. Qiu and B. Huang, Online pre-reduction of selenium(VI) with a newly designed UV/TiO$_2$ photocatalysis reduction device, *J. Anal. At. Spectrom.*, 2004, **19**, 715–716.

9 K. Chen, I. Hsu and Y.-C. Sun, Determination of methylmercury and inorganic mercury by coupling short-column ion chromatographic separation, on-line photocatalyst-assisted vapor generation, and inductively

coupled plasma mass spectrometry, *J. Chromatogr. A*, 2009, **1216**, 8933–8938.

10 C.-H. Lin, Y. Chen, Y.-A. Su, Y.-T. Luo, T.-T. Shih and Y.-C. Sun, Nanocomposite-coated microfluidic-based photocatalyst-assisted reduction device to couple high-performance liquid chromatography and inductively coupled plasma-mass spectrometry for online determination of inorganic arsenic species in natural water, *Anal. Chem.*, 2017, **89**, 5891–5899.

11 J. Jia, Z. Long, C. Zheng, X. Wu and X. Hou, Metal organic frameworks CAU-1 as new photocatalyst for photochemical vapor generation for analytical atomic spectrometry, *J. Anal. At. Spectrom.*, 2015, **30**, 339–342.

12 Z. Zou, J. Hu, F. Xu, X. Hou and X. Jiang, Nanomaterials for photochemical vapor generation analytical atomic spectrometry, *TrAC, Trends Anal. Chem.*, 2019, **114**, 242–250.

13 Y. Gao, M. Xu, R. Sturgeon, Z. Mester, Z. Shi, R. Galea, P. Saull and L. Yang, Metal ion-assisted photochemical vapor generation for the determination of lead in environmental samples by MC-ICPMS, *Anal. Chem.*, 2015, **87**, 4495–4502.

14 G. Chen, B. Lai, N. Mei, J. Liu and X. Mao, Mercury speciation by differential photochemical vapor generation at UV-B *vs.* UV-C wavelength, *Spectrochim. Acta, Part B*, 2017, **137**, 1–7.

15 J. Zhou, D. Deng, Y. Y. Su and Y. Lv, Determination of total inorganic arsenic in water samples by cadmium ion assisted photochemical vapor generation-atomic fluorescence spectrometry, *Microchem. J.*, 2019, **146**, 359–365.

16 J. Vyhnanovský, R. E. Sturgeon and S. Musil, Cadmium assisted photochemical vapor generation of tungsten for detection by ICPMS, *Anal. Chem.*, 2019, **91**, 13306–13312.

17 Y. Yu, Q. Zhao, H. L. Bao, Q. Mou, Z. M. Shi, Y. L. Chen and Y. Gao, Determination of trace bismuth in environmental waters by ICP-MS with cobalt ion-assisted photochemical vapour generation, *Geostand. Geoanal. Res.*, 2020, **44**, 617–627.

18 Q. Mou, L. Dong, L. Xu, Z. L. Song, Y. Yu, E. H. Wang, Y. H. Zhao and Y. Gao, Integration of cobalt ion assisted Fenton digestion and photochemical vapor generation: a green method for rapid determination of trace cadmium in rice, *J. Anal. At. Spectrom.*, 2021, **36**, 1422–1430.

19 Y. Yu, J. J. Hu, X. N. Zhao, J. C. Liu and Y. Gao, Photochemical vapor generation for germanium: synergistic effect from cobalt/chloride ions and air-liquid interfaces, *Anal. Bioanal. Chem.*, 2022, **414**, 5709–5717.

20 W. Zeng, J. Hu, H. J. Chen, Z. R. Zou, X. D. Hou and X. M. Jiang, Cobalt ion-enhanced photochemical vapor generation in a mixed acid medium for sensitive detection of tellurium(IV) by atomic fluorescence spectrometry, *J. Anal. At. Spectrom.*, 2020, **35**, 1405–1411.

21 W. Zeng, Z. H. Hu, J. Luo, X. D. Hou and X. M. Jiang, Highly sensitive determination of trace antimony in water samples by cobalt ion enhanced photochemical vapor generation coupled with atomic fluorescence spectrometry or ICP-MS, *Anal. Chim. Acta*, 2022, **1191**, 339361.

22 T. Xu, J. Hu and H. J. Chen, Transition metal ion Co(II)-assisted photochemical vapor generation of thallium for its sensitive determination by inductively coupled plasma mass spectrometry, *Microchem. J.*, 2019, **149**, 103972.

23 J. Hu, R. E. Sturgeon, K. Nadeau, X. D. Hou, C. Zheng and L. Yang, Copper ion assisted photochemical vapor generation of chlorine for its sensitive determination by sector field inductively coupled plasma mass spectrometry, *Anal. Chem.*, 2018, **90**, 4112–4118.

24 J. J. Hu, Y. Yu, Z. L. Xiao and Y. Gao, Photochemical vapor generation of zinc and gallium, *Microchem. J.*, 2023, **193**, 109178.

25 R. E. Sturgeon and E. Pagliano, Evidence for photochemical synthesis of fluoromethane, *J. Anal. At. Spectrom.*, 2020, **35**, 1720–1726.

26 R. M. de Oliveira, D. L. G. Borges, P. Grinberg and R. E. Sturgeon, High-efficiency photoreductive vapor generation of osmium, *J. Anal. At. Spectrom.*, 2021, **36**, 2097–2106.

27 Y. L. Wang, L. L. Lin, J. Liu, X. F. Mao, J. H. Wang and D. U. Qin, Ferric ion induced enhancement of ultraviolet vapour generation coupled with atomic fluorescence spectrometry for the determination of ultratrace inorganic arsenic in surface water, *Analyst*, 2016, **141**, 1530–1536.

28 Y. Yu, Y. Jia, Z. Shi, Y. Chen, S. Ni, R. Wang, Y. Tang and Y. Gao, Enhanced photochemical vapor generation for the determination of bismuth by inductively coupled plasma mass spectrometry, *Anal. Chem.*, 2018, **90**, 13557–13563.

29 H. Y. He, X. H. Peng, Y. Yu, Z. M. Shi, M. Xu, S. J. No and Y. Gao, Photochemical vapor generation of tellurium: synergistic effect from ferric ion and nano-TiO$_2$, *Anal. Chem.*, 2018, **90**, 5737–5743.

30 J. Šoukal, R. E. Sturgeon and S. Musil, Efficient photochemical vapor generation of molybdenum for ICPMS detection, *Anal. Chem.*, 2018, **90**, 11688–11695.

31 E. Nováková, K. Horová, V. Červený, J. Hraníček and S. Musil, UV photochemical vapor generation of Cd from a formic acid based medium: optimization, efficiency and interferences, *J. Anal. At. Spectrom.*, 2020, **35**, 1380–1388.

32 L. Dong, H. J. Chen, Y. Y. Ning, Y. W. He, Y. Yu and Y. Gao, Vanadium species-assisted photochemical vapor generation for direct detection of trace tellurium, *Anal. Chem.*, 2022, **94**, 4770–4778.

33 X. Deng, L. Dong, H. Chen, W. Wang, Y. Yu and Y. Gao, Sensitive determination of arsenic by photochemical vapor generation with inductively coupled plasma mass spectrometry: synergistic effect from antimony and cadmium, *Anal. Chem.*, 2024, **96**, 652–660.

34 Q. Yang, H. Chen, J. Hu, K. Huang and X. Hou, Simultaneous detection of ruthenium and osmium by photochemical vapor generation-inductively coupled plasma-mass spectrometry, *Anal. Chem.*, 2022, **94**, 593–599.

35 S. Musil, J. R. Vyhnanovský and R. E. Sturgeon, Ultrasensitive detection of ruthenium by coupling cobalt and cadmium ion-assisted photochemical vapor generation to inductively coupled plasma mass spectrometry, *Anal. Chem.*, 2021, **93**, 16543–16551.

This journal is © The Royal Society of Chemistry 2025

J. Anal. At. Spectrom., 2025, **40**, 70–97 | **93**

36 S. Musil, E. Jeníková, J. R. Vyhnanovský and R. E. Sturgeon, Highly efficient photochemical vapor generation for sensitive determination of iridium by inductively coupled plasma mass spectrometry, *Anal. Chem.*, 2023, **95**, 3694–3702.

37 F. Xu, Z. Zou, J. He, M. Li, K. Xu and X. Hou, In situ formation of nano-CdSe as a photocatalyst: cadmium ion-enhanced photochemical vapour generation directly from Se(VI), *Chem. Commun.*, 2018, **54**, 4874–4877.

38 R. M. de Oliveira, D. L. G. Borges, P. Grinberg, Z. Mester and R. E. Sturgeon, Copper-ion assisted photochemical vapor generation of bromide and bromate, *J. Anal. At. Spectrom.*, 2021, **36**, 1235–1243.

39 J. M. Carraher, O. Pestovsky and A. Bakac, Transition metal ion-assisted photochemical generation of alkyl halides and hydrocarbons from carboxylic acids, *Dalton Trans.*, 2012, **41**, 5974–5980.

40 A. Bakac, Effects of halide ions and carbon monoxide on the reactions of iron(III) with alkyl radicals, *Croat. Chem. Acta*, 2001, **74**, 633–640.

41 R. Ge, Z. Xu, K. Yang and H. Ge, Transition-metal-catalyzed C(sp^3)-H bond fluorination reactions, *Chem Catal.*, 2024, **4**, 101009.

42 G. Ferraudi, Photochemical generation of metastable methylcopper complexes. Oxidation-reduction of methyl radicals by copper complexes, *Inorg. Chem.*, 1978, **17**, 2506–2508.

43 A. W. Adamson, W. L. Waltz, E. Zinato, D. W. Watts, P. D. Fleischauer and R. D. Lindholm, Photochemistry of transition-metal coordination compounds, *Chem. Rev.*, 1968, **68**, 541–585.

44 P. Ciesla, P. Kocot, P. Mytych and Z. Stasicka, Homogeneous photocatalysis by transition metal complexes in the environment: a review, *J. Mol. Catal. A: Chem.*, 2004, **224**, 17–33.

45 J. Hu, H. Chen, X. Hou and X. Jiang, Cobalt and copper ions synergistically enhanced photochemical vapor generation of molybdenum: mechanism study and analysis of water samples, *Anal. Chem.*, 2019, **91**, 5938–5944.

46 J. Hu, C. Li, Y. Zhen, H. Chen, J. He and X. Hou, Current advances of chemical vapor generation in nontetrahydroborate media for analytical atomic spectrometry, *Trends Anal. Chem.*, 2022, **155**, 116677.

47 L. L. Perissinotti, M. A. Brusa and M. A. Grela, Yield of carboxyl anion radicals in their photocatalytic degradation of formate over TiO$_2$ particles, *Langmuir*, 2001, **17**, 8422–8427.

48 M. Kaise, H. Nagai, K. Tokuhashi and S. Kondo, Electron spin resonance studies of photocatalytic interface reactions of suspended M/TiO$_2$ (M = Pt, Pd, Ir, Rh, Os or Ru) with alcohol and acetic acid in aqueous media, *Langmuir*, 1994, **10**, 1345–1347.

49 P. C. Ford, From curiosity to applications. A personal perspective on inorganic photochemistry, *Chem. Sci.*, 2016, **7**, 2964–2986.

50 T. Suzuki, R. E. Sturgeon, C. Zheng, A. Hioki, H. Tao and T. Nakazato, Influence of speciation on response from

51 R. E. Sturgeon, Quantitation of bromine by ICP-ToF-MS following photochemical vapor generation, *Anal. Chem.*, 2015, **87**, 3072–3079.

52 H. Coutinho de Jesus, P. Grinberg and R. E. Sturgeon, System optimization for determination of cobalt in biological samples by ICP-OES using photochemical vapor generation, *J. Anal. At. Spectrom.*, 2016, **31**, 1590–1604.

53 G. V. Buxton and R. M. Sellers, The radiation chemistry of metal ions in aqueous solution, *Coord. Chem. Rev.*, 1977, **22**, 195–274.

54 M. G. Gonzalez, E. Oliveros, M. Worner and A. M. Braun, Vacuum-ultraviolet photolysis of aqueous reaction systems, *J. Photochem. Photobiol., C*, 2004, **5**, 225–246.

55 J. A. Kloepfer, V. H. Vilchiz, V. A. Lenchenkov, A. C. Germaine and S. E. Bradforth, The ejection distribution of solvated electrons generated by the one-photon photodetachment of aqueous I⁻ and two photon ionization of the solvent, *J. Chem. Phys.*, 2000, **113**, 6288–6307.

56 K. Zoschke, H. Börnick and E. Worch, Vacuum-UV radiation at 185 nm in water treatment – a review, *Water Res.*, 2014, **52**, 131–145.

57 J. Zechner and N. Getoff, Photoproduction of hydrated electrons from formate ions at 184.9 nm, *Int. J. Radiat. Phys. Chem.*, 1974, **6**, 215–218.

58 G. Imoberdorf and M. Mohseni, Modeling and experimental evaluation of vacuum-UV photoreactors for water treatment, *Chem. Eng. Sci.*, 2011, **66**, 1159–1167.

59 G. V. Buxton and R. M. Sellers, Acid dissociation constant of the carboxyl radical. Pulse radiolysis studies of aqueous solutions of formic acid and sodium formate, *J. Chem. Soc., Faraday Trans. 1*, 1973, **69**, 555–559.

60 G. E. Adams and E. J. Hart, Radiolysis and photolysis of aqueous formic acid. Carbon monoxide formation, *J. Am. Chem. Soc.*, 1962, **84**, 3994–3999.

61 E. J. Hart, Mechanism of the γ-ray induced oxidation of formic acid in aqueous solution, *J. Am. Chem. Soc.*, 1951, **73**, 68–73.

62 J. Hu, C. Li, H. Chen and X. Hou, Photochemical hydride generation in sulfite medium: sample introduction into an inductively coupled plasma mass spectrometer for the determination of ultratrace inorganic arsenic, *Anal. Chem.*, 2023, **95**, 10498–10503.

63 E. Jeníková, J. Vyhnanovský, K. Hašlová, R. E. Sturgeon and S. Musil, Efficient photochemical vapor generation from low concentration formic acid media, *Anal. Chem.*, 2024, **96**, 1241–1250.

64 A. J. Allmand and L. Reeve, The photochemical decomposition of aqueous formic acid solutions, *J. Chem. Soc.*, 1926, **129**, 2852–2863.

65 H. Su, Y. He and F. Konga, Photodissociation of formic acid, *J. Chem. Phys.*, 2000, **113**, 1891–1897.

66 J. Thøgersen, S. K. Jensen, O. Christiansen and S. R. Keiding, Fast photodynamics of aqueous formic acid, *J. Phys. Chem. A*, 2004, **108**, 7483–7489.

94 | *J. Anal. At. Spectrom.*, 2025, **40**, 70–97

This journal is © The Royal Society of Chemistry 2025

67 M. Burton, The photolysis of acetic acid, *J. Am. Chem. Soc.*, 1936, **58**, 692.

68 P. Ausloos and E. W. R. Steacie, The vapor phase photolysis of acetic acid, *Can. J. Chem.*, 1955, **33**, 1530–1535.

69 J. L. Wilkerson and W. A. Guillory, Condensed phase photochemistry of acetic acid in the vacuum UV, *J. Photochem.*, 1977, **7**, 261.

70 L. J. Mittal, J. P. Mittal and E. Hayon, Photo-induced decarboxylation of aliphatic acids and esters in solution. Dependence upon state of protonation of the carboxyl group, *J. Phys. Chem.*, 1973, **77**, 1482–1487.

71 S. Hamid, I. Ivanova, T. H. Jeon, R. Dillert, W. Choi and D. W. Bahnemann, Photocatalytic conversion of acetate into molecular hydrogen and hydrocarbons over Pt/TiO$_2$: pH dependent formation of Kolbe and Hofer-Moest products, *J. Catal.*, 2017, **349**, 128–135.

72 R. Chelli, R. Righini and S. Califano, Structure of liquid formic acid investigated by first principle and classical molecular dynamics simulations, *J. Phys. Chem. B*, 2005, **109**, 17006–17013.

73 R. Bar-Ziv, I. Zilbermann, T. Zidki, G. Yardeni, V. Shevchenko and D. Meyerstein, Coating Pt^0 nanoparticles with methyl groups: the reaction between methyl radicals and Pt^0 NPs suspended in aqueous solutions, *Chem.–Eur. J.*, 2012, **18**, 6733–6736.

74 R. Bar-Ziv, I. Zilbermann, O. Oster-Golberg, T. Zidki, G. Yardeni, H. Cohen and D. Meyerstein, On the lifetime of the transients (NP)-(CH$_3$)$_n$ (NP=Ag^0, Au^0, TiO$_2$ nanoparticles) formed in the reactions between methyl radicals and nanoparticles suspended in aqueous solutions, *Chem.–Eur. J.*, 2012, **18**, 4699–4705.

75 M. König, J. Vaes, E. Klemm and D. Pant, Solvents and Supporting Electrolytes in the Electrocatalytic Reduction of CO$_2$, *iScience*, 2019, **19**, 135–160.

76 R. Sander, Compilation of Henry's law constants (version 4.0) for water as solvent, *Atmos. Chem. Phys.*, 2015, **15**, 4399–4981.

77 Y. Gao, R. E. Sturgeon, Z. Mester, X. Hou, C. Zheng and L. Yang, Direct determination of trace antimony in natural waters by photochemical vapor generation ICPMS: method optimization and comparison of quantitation strategies, *Anal. Chem.*, 2015, **87**, 7996–8004.

78 R. M. de Oliveira and D. L. G. Borges, UV photochemical vapor generation of noble metals (Au, Ir, Pd, Pt and Rh): a feasibility study using inductively coupled plasma mass spectrometry and seawater as a test matrix, *J. Anal. At. Spectrom.*, 2018, **33**, 1700–1706.

79 P. Grinberg and R. E. Sturgeon, Photochemical vapor generation of iodine for detection by ICP-MS, *J. Anal. At. Spectrom.*, 2009, **24**, 508–514.

80 C. Zheng, R. E. Sturgeon and X. Hou, UV photochemical vapor generation and *in situ* preconcentration for determination of ultra-trace nickel by flow injection graphite furnace atomic absorption spectrometry, *J. Anal. At. Spectrom.*, 2009, **24**, 1452–1458.

81 H. Duan, Z. Gong and S. Yang, Online photochemical vapour generation of inorganic tin for inductively coupled plasma mass spectrometric detection, *J. Anal. At. Spectrom.*, 2015, **30**, 410–416.

82 L. Dong, W. Wang, Y. Ning, X. Deng and Y. Gao, Detection of trace antimony by vanadium (IV) ion assisted photochemical vapor generation with inductively coupled plasma mass spectrometry measurement, *Anal. Chim. Acta*, 2023, **1251**, 341006.

83 E. Jeníková, E. Nováková, J. Hraníček and S. Musil, Ultra-sensitive speciation analysis of tellurium by manganese and iron assisted photochemical vapor generation coupled to ICP-MS/MS, *Anal. Chim. Acta*, 2022, **1201**, 339634.

84 S. Li, Y. Gao, Y. Yu, H. He, X. Hu, S. Ni, Z. Shi, X. Peng and R. Liu, Direct determination of trace lead in seawater by inductively coupled plasma mass spectrometry after photochemical vapor generation, *At. Spectrosc.*, 2017, **38**, 37–43.

85 J. L. Weeks, G. M. A. C. Meaburn and S. Gordon, Absorption coefficients of liquid water and aqueous solutions in the far ultraviolet, *Radiat. Res.*, 1963, **19**, 559–567.

86 I. Janik and G. N. R. Tripathi, The nature of the CO$_2^-$ radical anion in water, *J. Chem. Phys.*, 2016, **144**, 154307.

87 S. Mozia, A. Heciak and A. W. Morawski, Photocatalytic acetic acid decomposition leading to the production of hydrocarbons and hydrogen on Fe-modified TiO$_2$, *Catal. Today*, 2011, **161**, 189–195.

88 Y. Jia, Q. Mou, Y. Yu, Z. Shi, Y. Huang, S. Ni, R. Wang and Y. Gao, Reduction of interferences using Fe-containing metal–organic frameworks for matrix separation and enhanced photochemical vapor generation of trace bismuth, *Anal. Chem.*, 2019, **91**, 5217–5224.

89 G. B. Porter and S. W. Benson, The reaction of carbon monoxide with free radicals, *J. Am. Chem. Soc.*, 1953, **75**, 2773–2774.

90 H. A. Schwarz and A. J. Salzman, The radiation chemistry of aqueous nitrite solutions: the hydrogen peroxide yield, *Radiat. Res.*, 1958, **9**, 502–508.

91 A. J. Elliot and F. C. Sopchyshyn, The radiolysis at room temperature and 118 °C of aqueous solutions containing sodium nitrate and either sodium formate or 2-propanol, *Can. J. Chem.*, 1983, **61**, 1578–1582.

92 G. L. Hug, D. M. Camaioni and I. Carmichael, EPR detection of HNO$_2^-$ in the radiolysis of aqueous nitrite and quantum chemical calculation of its stability and hyperfine parameters, *J. Phys. Chem. A*, 2004, **108**, 6599–6604.

93 J. Jortner, M. Ottolenghi and G. Stein, On the photochemistry of aqueous solutions of chloride, bromide and iodide ions, *J. Phys. Chem.*, 1964, **68**, 247–255.

94 U. Shuali, M. Ottolenghi, J. Rabani and Z. Yelin, On the photochemistry of aqueous nitrate solutions excited in the 195 nm band, *J. Phys. Chem.*, 1969, **73**, 3445–3451.

95 M. Daniels, R. V. Meyers and E. V. Belardo, Photochemistry of the aqueous nitrate system. I. Excitation in the 300-m.mu. band, *J. Phys. Chem.*, 1968, **72**, 389–399.

This journal is © The Royal Society of Chemistry 2025

J. Anal. At. Spectrom., 2025, **40**, 70–97 | 95

96 X. Guo, R. E. Sturgeon, Z. Mester and G. J. Gardner, UV Vapor generation for determination of Se by heated quartz tube AAS, *Anal. Chem.*, 2003, **75**, 2092–2099.

97 G. S. Lopes, R. E. Sturgeon, P. Grinberg and E. Pagliano, Evaluation of approaches to the abatement of nitrate interference with photochemical vapor generation, *J. Anal. At. Spectrom.*, 2017, **32**, 2378–2390.

98 M. Rybínová, V. Červený, J. Hraníček and P. Rychlovský, UV-photochemical vapor generation with quartz furnace atomic absorption spectrometry for simple and sensitive determination of selenium in dietary supplements, *Microchem. J.*, 2016, **124**, 584–593.

99 J. Vyhnanovský, D. Yildiz, B. Stadlerov and S. Musil, Efficient photochemical vapor generation of bismuth using a coiled teflon reactor: Effect of metal sensitizers and analytical performance with flame-in-gas-shield atomizer and atomic fluorescence spectrometry, *Microchem. J.*, 2021, **164**, 105997.

100 M. Kozlowski and T. Yoon, Editorial for the special issue on photocatalysis, *J. Org. Chem.*, 2016, **81**, 6895–6897.

101 H. Bao, X. Peng, Z. Song, Y. Ning, Y. Yu and Y. Gao, Natural mineral assisted photochemical vapor generation for determination of trace inorganic arsenic by inductively coupled plasma mass spectrometry, *Microchem. J.*, 2021, **170**, 106689.

102 R. E. Sturgeon, *Unpublished Results; Presented at the 16th Rio Symposium on Atomic Spectrometry*, Bento Goncalves, Brazil, November 28-30, 2023.

103 F. Laborda, A. C. Gimenez-Ingalaturre, E. Bolea and J. R. Castillo, About detectability and limits of detection in single particle inductively coupled plasma mass spectrometry, *Spectrochim. Acta, Part B*, 2020, **169**, 105883.

104 S. Lee, X. Bi, R. B. Reed, J. F. Ranville, P. Herckes and P. Westerhoff, Nanoparticle size detection limits by single particle ICP-MS for 40 elements, *Environ. Sci. Technol.*, 2014, **48**, 10291–10300.

105 L. Liu, X. Zhang, L. Yang, L. Ren, D. Wang and J. Ye, Metal nanoparticles induced photocatalysis, *Natl. Sci. Rev.*, 2017, **4**, 761–780.

106 J. Zhao, S. C. Nguyen, R. Ye, B. Ye, H. Weller, G. A. Somorjai, A. P. Alivisatos and F. D. Toste, A comparison of photocatalytic activities of gold nanoparticles following plasmonic and interband excitation and a strategy for harnessing interband hot carriers for solution phase photocatalysis, *ACS Cent. Sci.*, 2017, **3**, 482–488.

107 H. Huang, K. A. Steiniger and T. H. Lambert, Electrophotocatalysis: combining light and electricity to catalyze reactions, *J. Am. Chem. Soc.*, 2022, **144**, 12567–12583.

108 L. Zhang, M. Zhang, X. Guo, X. Liu, P. Kang and X. Chen, Sorption characteristics and separation of tellurium ions from aqueous solutions using nano-TiO$_2$, *Talanta*, 2010, **83**, 344–350.

109 V. Nguyen, D. Beydoun and R. Amal, Photocatalytic reduction of selenite and selenate using TiO$_2$ photocatalyst, *J. Photochem. Photobiol., A*, 2005, **171**, 113–120.

110 Z. Zou, Y. Zhen, C. Zheng and X. Hou, "Catalysts in photochemical vapor generation" in *Vapor Generation Techniques for Trace Element Analysis: Fundamental Aspects*, ed A. D'Ulivo and R. E. Sturgeon, Elsevier, 2022, Chapter 8.

111 K. An and G. A. Somorjai, Nanocatalysis I: Synthesis of metal and bimetallic nanoparticles and porous oxides and their catalytic reaction studies, *Catal. Lett.*, 2015, **145**, 233–248.

112 P. V. Kamat, Photophysical, photochemical and photocatalytic aspects of metal nanoparticles, *J. Phys. Chem. B*, 2002, **106**, 7729–7744.

113 J. A. Adekoya, K. O. Ogunniran, T. O. Siyanbola, E. O. Dare and N. Revaprasadu, "Band structure, morphology, functionality, and size dependent properties of metal nanoparticles", in *Noble and Precious Metals - Properties, Nanoscale Effects and Applications*, M. Seehra and A. D. Bristow (Eds), Chapter 2, IntechOpen, 2018, pp. 15 - 42. ISBN: 978-1-78923-293-6.

114 P. Han, W. Martens, E. R. Waclawik, S. Sarina and H. Zhu, Metal nanoparticle photocatalysts: synthesis, characterization and application, *Part. Part. Syst. Charact.*, 2018, **35**, 1700489.

115 A. Krishnan, A. Swarnalal, D. Das, M. Krishnan, V. S. Saji and S. M. A. Shibli, A review on transition metal oxides based photocatalysts for degradation of synthetic organic pollutants, *J. Environ. Sci.*, 2024, **139**, 389–417.

116 H. Xu, Q.-Y. Wang, M. Jiang and S. Li, Application of valence-variable transition-metal-oxide-based nanomaterials in electrochemical analysis: A review, *Anal. Chim. Acta*, 2024, **1295**, 342270.

117 A. M. Abu-Dief, Development of metal oxide nanoparticles as semiconductors, *Nanomater. Nanotechnol.*, 2020, **1**, 5–10.

118 K. Roy, C. K. Sarkar and C. K. Ghosh, Photocatalytic activity of biogenic silver nanoparticles synthesized using potato (*Solanum tuberosum*) infusion, *Spectrochim. Acta, Part A*, 2015, **146**, 286–291.

119 R. Narayanan and M. A. El-Sayed, Catalysis with transition metal nanoparticles in colloidal solution: nanoparticle shape dependence and stability, *J. Phys. Chem. B*, 2005, **109**, 12663–12676.

120 A. A. Ponce and K. J. Klabunde, Chemical and catalytic activity of copper nanoparticles prepared *via* metal vapor synthesis, *J. Mol. Catal. A: Chem.*, 2005, **225**, 1–6.

121 M. A. El-Sayed, J. Yu, G. Liu and M. Jaroniec, Non-noble plasmonic metal-based photocatalysts, *Chem. Rev.*, 2022, **122**, 10484–10537.

122 J. Twilton, C. Le, P. Zhang, M. H. Shaw, R. W. Evans and D. W. C. MacMillan, The merger of transition metal and photocatalysis, *Nat. Rev. Chem.*, 2017, **1**, 1–17.

123 F. Kraushofer and G. S. Parkinson, Single-atom catalysis: insights from model systems, *Chem. Rev.*, 2022, **122**, 14911–14939.

124 S. K. Kaiser, Z. Chen, D. F. Akl, S. Mitchell and J. Pérez-Ramírez, Single-atom catalysts across the Periodic Table, *Chem. Rev.*, 2020, **120**, 11703–11809.

96 | *J. Anal. At. Spectrom.*, 2025, **40**, 70–97

This journal is © The Royal Society of Chemistry 2025

125 L. Xiangdong, W. Jia, N. Chao, X. Yongjie and L. Fuwei, Manipulating the structure of metal at atomic level to enhance the catalytic performance, *Chem Catal.*, 2024, **4**, 100810.

126 Y. Huang, J. Hou, L. Zhan, Q. Zhang, W. Tang and B. Li, Photoredox activation of formate salts: hydrocarboxylation of alkenes *via* carboxyl group transfer, *ACS Catal.*, 2021, **11**, 15004–15012.

127 M. Biegel, T. Schikarski, P. C. Lopez, L. Gromotka, C. Lübbert, A. Völkl, C. Damm, J. Walter and W. Peukert, Efficient quenching sheds light on early stages of gold nanoparticle formation, *RSC Adv.*, 2023, **13**, 18001–18013.

128 K. Cao, J. Biskupek, C. T. Stoppiello, R. L. McSweeney, T. W. Chamberlain, Z. Liu, K. Suenaga, S. T. Skowron, E. Besley, A. N. Khlobystov and U. Kaiser, Atomic mechanism of metal crystal nucleus formation in a single-walled carbon nanotube, *Nat. Chem.*, 2020, **12**, 921–928.

129 B. Huang, Y. Liu, H. Kobayashi, Z. Tan, T. Yamamato, T. Toriyama, S. Matsumura, S. Kawaguchi, Y. Kubota, H. Zheng and H. Kitagawa, Cu_xRu_{1-x} catalysts for carbon neutralization with CH_4 or CO production, *Chem Catal.*, 2023, **3**, 100705.

130 T. S. Rodrigues, A. G. M. da Silva and P. H. C. Camargo, Nanocatalysis by noble metal nanoparticles: controlled synthesis for the optimization and understanding of activities, *J. Mater. Chem. A*, 2019, **7**, 5857–5874.

131 J. Ma, X. Tan, Q. Zhang, Y. Wang, J. Zhang and L. Wang, Exploring the size effect of Pt nanoparticles on the photocatalytic nonoxidative coupling of methane, *ACS Catal.*, 2021, **11**, 3352–3360.

132 R. Zhang, L. Song and B. Wang, The interaction mechanism of CO_2 with CH_3 and H on Cu {111} surface in synthesis of acetic acid from CH_4/CO_2: A DFT study, *Appl. Catal., A*, 2012, **443–444**, 50–58.

133 G. R. Dey, K. N. R. Nair and K. K. Pushpa, Photolysis studies on HCOOH and $HCOO^-$ in presence of TiO_2 photocatalyst as suspension in aqueous medium, *J. Nat. Gas Chem.*, 2009, **18**, 50–54.

134 P. J. Wyatt, Differential light scattering and the measurement of molecules and nanoparticles: A review, *Anal. Chim. Acta: X*, 2021, **7–8**, 100070.

135 H. Kato, A. Nakamura, K. Takahashi and S. Kinugasa, Accurate size and size-distribution determination of polystyrene latex nanoparticles in aqueous medium using dynamic light scattering and asymmetrical flow field flow fractionation with multi-angle light scattering, *Nanomaterials*, 2012, **2**, 15–30.

136 Y. Matsuura, N. Ouchi, A. Nakamura and H. Kato, Determination of an accurate size distribution of nanoparticles using particle tracking analysis corrected for the adverse effect of random Brownian motion, *Phys. Chem. Chem. Phys.*, 2018, **20**, 17839–17846.

137 W.-M. Cheng and R. Shang, Transition metal-catalyzed organic reactions under visible light: recent developments and future perspectives, *ACS Catal.*, 2020, **10**, 9170–9196.

138 S. De Kreijger, F. Glaser and L. Troian-Gautier, From photons to reactions: key concepts in photoredox catalysis, *Chem Catal.*, 2024, DOI: **10.1016/ j.checat.2024.101110**.

139 H. Sato and T. Sugimoto, Direct *operando* identification of reactive electron species driving photocatalytic hydrogen evolution on metal-loaded oxides, *J. Am. Chem. Soc.*, 2024, **146**, 24800–24807.

140 Z. Zou, Y. Tian, W. Zeng, X. Hou and X. Jiang, Effect of variable ultraviolet wavelength and intensity on photochemical vapor generation of trace selenium detected by atomic fluorescence spectrometry, *Microchem. J.*, 2018, **140**, 189–195.

This journal is © The Royal Society of Chemistry 2025

J. Anal. At. Spectrom., 2025, **40**, 70–97 | **97**